ELSEVIER

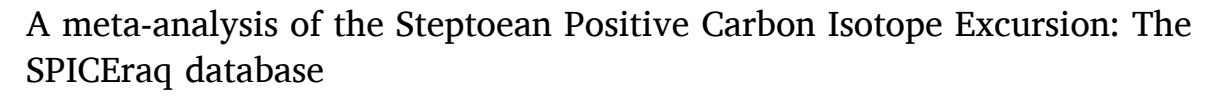
Contents lists available at ScienceDirect

# **Earth-Science Reviews**

journal homepage: www.elsevier.com/locate/earscirev



## Review article





Mikaela A. Pulsipher <sup>a</sup>, James D. Schiffbauer <sup>a,b,\*</sup>, Matthew J. Jeffrey <sup>c,a</sup>, John Warren Huntley <sup>a</sup>, David A. Fike <sup>d</sup>, Kevin L. Shelton <sup>a</sup>

- <sup>a</sup> Department of Geological Sciences, University of Missouri, Columbia, MO 65211, USA
- <sup>b</sup> X-ray Microanalysis Core Facility, University of Missouri, Columbia, MO 65211, USA
- <sup>c</sup> Department of Environmental Studies, Bellarmine University, Louisville, KY 40205, USA
- d Department of Earth and Planetary Sciences, Washington University in St. Louis, St. Louis, MO 63130, USA

## ARTICLE INFO

#### Keywords:

Steptoean Positive Carbon Isotope Excursion Isotope geochemistry Chemostratigraphy Cambrian Period Furongian Series Paibian Stage

## ABSTRACT

The Steptoean Positive Isotopic Carbon Excursion (SPICE) is a prominent chemostratigraphic feature in the Lower Paleozoic. It has been used to correlate Upper Cambrian carbonate strata globally, and is cited as intimately linked to the Crepicephalus-Aphelaspis trilobite extinction event and the Sauk II-Sauk III megasequence transition. Despite the global nature of the SPICE event, regional/local conditions serve as a control on the expression of the SPICE event in the rock record. In light of this, and to better understand how reliable the SPICE event is as a chemostratigraphic tool for correlation, we have created the "SPICEraq," a database comprising 78 SPICE-bearing sections containing 6669 individual  $\delta^{13}$ C analyses. In this study, we quantitatively evaluate the variability in SPICE records, and document that, while the excursion is a global signature, its stratigraphic expression is influenced by such conditions as paleolatitude, paleocontinent, water depth, and facies. While the magnitude of the SPICE excursion is generally consistent (an  $\sim$ 4% increase), the peak  $\delta^{13}$ C values are quite variable (ranging from +0.35 to +5.87%). Specifically, sections located between 30 and  $60^{\circ}$ S paleolatitude ca. 500 Ma record  $\delta^{13}$ C values  $\sim$ 1 to 2‰ lower than those from lower paleolatitudes. Sections deposited in shallow water depths and facies also record lower  $\delta^{13}$ C values than intermediate and deep-water facies; the deep-water facies exhibit the most  $^{13}$ C-enriched carbonates at the peak of the SPICE and post-excursion. The stratigraphic thickness of the excursion varies widely, ranging from <3 to ~884 m, and is significantly impacted by all categorical variables investigated in this study. This study documents that the rising limb of the SPICE is immediately preceded by a small negative  $\delta^{13}$ C excursion in 75% of sections with data collected pre-SPICE. While 32% of sections record a  $\delta^{13}$ C plateau during peak SPICE, its presence in the  $\delta^{13}$ C record does not appear to be influenced by any environmental conditions investigated herein. Altogether, these analyses indicate that regional/local conditions impact the stratigraphic expression of  $\delta^{13}$ C records, and thus care should be taken to use robust, quantitative measures to compare and correlate excursions.

# 1. Introduction

The carbon isotope record of the Cambrian Period ( $\sim$ 540–485 Ma) shows considerable variation. Through the first two Cambrian Series ( $\sim$ 540–497 Ma), fluctuating positive and negative excursions are common and characteristic (Maloof et al., 2005; Dilliard et al., 2007; Saltzman and Thomas, 2012). Following the end of Series 2, the  $\delta^{13}C_{carb}$  record stabilizes around 0‰ V-PDB (Vienna Pee Dee Belemnite

standard; hereafter,  $\delta^{13}$ C refers to carbonate carbon), and is punctuated, mostly, by only lower magnitude excursions. The exception is the prominent Steptoean Positive Isotopic Carbon Excursion (SPICE) event near the Guzhangian–Paibian Stage boundary (which also corresponds to the North American Marjuman–Steptoean Stage boundary and the Miaolingian–Furongian Series boundary; Fig. 1) (Saltzman et al., 2000; Saltzman and Thomas, 2012; Zhao et al., 2019).

First named by Saltzman et al. (1998), the SPICE is a  $\sim$ 4 to 5%

<sup>\*</sup> corresponding author at: Department of Geological Sciences, University of Missouri, Columbia, MO 65211, USA

E-mail addresses: mpbg6@mail.missouri.edu (M.A. Pulsipher), schiffbauerj@missouri.edu (J.D. Schiffbauer), mjeffrey@bellarmine.edu (M.J. Jeffrey), huntleyj@

missouri.edu (J.W. Huntley), dfike@levee.wustl.edu (D.A. Fike), sheltonkl@missouri.edu (K.L. Shelton).

increase in  $\delta^{13}$ C values that has been used in global chemostratigraphic correlation. The SPICE has been documented in carbonate stratigraphic sections around the world, including North America (e.g., Saltzman et al., 1998; Hurtgen et al., 2009), South America (e.g., Sial et al., 2008), Europe (e.g., Pruss et al., 2019; Álvaro et al., 2008), Asia (e.g., Kouchinsky et al., 2008; Ng et al., 2014; Lim et al., 2015; Wotte and Strauss, 2015), and Australia (e.g., Schmid et al., 2018). With such a broad geographic occurrence of this pronounced excursion, the inference commonly adopted is that the SPICE represents a global perturbation of the carbon cycle (Saltzman et al., 1998). Further, not only has the excursion been identified in both shallow and deep water carbonates (Saltzman et al., 2000; Glumac and Mutti, 2007; Zuo et al., 2018), but also in a smaller magnitude excursion (+1 to +2%) of organic carbon isotope values ( $\delta^{13}C_{org}$ ) from organic-rich shales (Álvaro et al., 2008; Ahlberg et al., 2009; Ahlberg et al., 2019; Baker, 2010; Saltzman et al., 2011; Woods et al., 2011).

Other geochemical analyses have been utilized to investigate the SPICE event, including oxygen, sulfur, and uranium isotopes, as well as other elemental proxies (e.g., Elrick et al., 2011; Gill et al., 2011; Dahl et al., 2014; Wotte and Strauss, 2015; LeRoy and Gill, 2019). Unlike  $\delta^{13}C$  values,  $\delta^{18}O$  values do not show a consistent global pattern. In some sections,  $\delta^{18}O$  has an inverse relationship with  $\delta^{13}C$ , with the nadir of  $\delta^{18}O$  values corresponding to the peak  $\delta^{13}C$  values (Elrick et al., 2011). In other cases,  $\delta^{18}O$  values covary with  $\delta^{13}C$  and record a positive  $\delta^{18}O$  excursion, such as in the Kyrshabakty section in Kazakhstan (+1% V-PDB) (Wotte and Strauss, 2015) and the Kulyumbe section in Siberia (+4% V-PDB) (Kouchinsky et al., 2008). In many instances, however,  $\delta^{18}O$  does not covary with  $\delta^{13}C$  and may be virtually invariant through the SPICE, such as in multiple boreholes from Australia (Schmid, 2017),

the Tangwangzhai section in China (Zhu et al., 2004), and the Shingle Pass section in Nevada, United States (Baker, 2010). A positive  $\delta^{34}$ S excursion of varying amplitudes has also been shown to correlate with the SPICE in multiple sections around the globe (Hurtgen et al., 2009; Gill et al., 2011; Saltzman et al., 2011; Wotte and Strauss, 2015; LeRoy and Gill, 2019). Dahl et al. (2014) measured uranium isotopes in the Mt. Whelan core from Australia to further investigate the relationship between the SPICE event and possible euxinia. Iron, mercury, and molybdenum concentrations have been analyzed to evaluate the paleoredox conditions of SPICE occurrences in North America (LeRoy and Gill, 2019), Sweden (Gill et al., 2011), and Scotland (Pruss et al., 2019). Results from these studies suggest that the timing of anoxic and/ or euxinic conditions in different sections is variable with respect to trilobite extinctions and peak  $\delta^{13}$ C values of the SPICE (Gill et al., 2011; Dahl et al., 2014; LeRoy and Gill, 2019; Pruss et al., 2019). Additionally. phosphatic brachiopods from Laurentia display δ<sup>13</sup>C values preserving the SPICE event in a manner similar to that of corresponding bulk carbonate analyses (Cowan et al., 2005; Auerbach, 2004; Elrick et al.,

The SPICE event may have also been biologically important. It occurred coincidentally with a trilobite biomere turnover, but whether it was causally or only temporally linked remains a question (Saltzman et al., 1998, 2000; Gill et al., 2011; Gerhardt, 2014; Gerhardt and Gill, 2016; Schiffbauer et al., 2017). The onset of the rising limb is coincident with the first appearance datum (FAD) of the trilobite *Glyptagnostus reticulatus* and the base of the Pterocephaliid biomere (Fig. 1; Saltzman et al., 2000; Glumac, 2011). The FAD of *G. reticulatus* is also correlative with the base of the *Aphelaspis* zone following the two-phase extinction of *Crepicephalus*-zone and *Coosella perplexa*-subzone trilobites (Glumac,

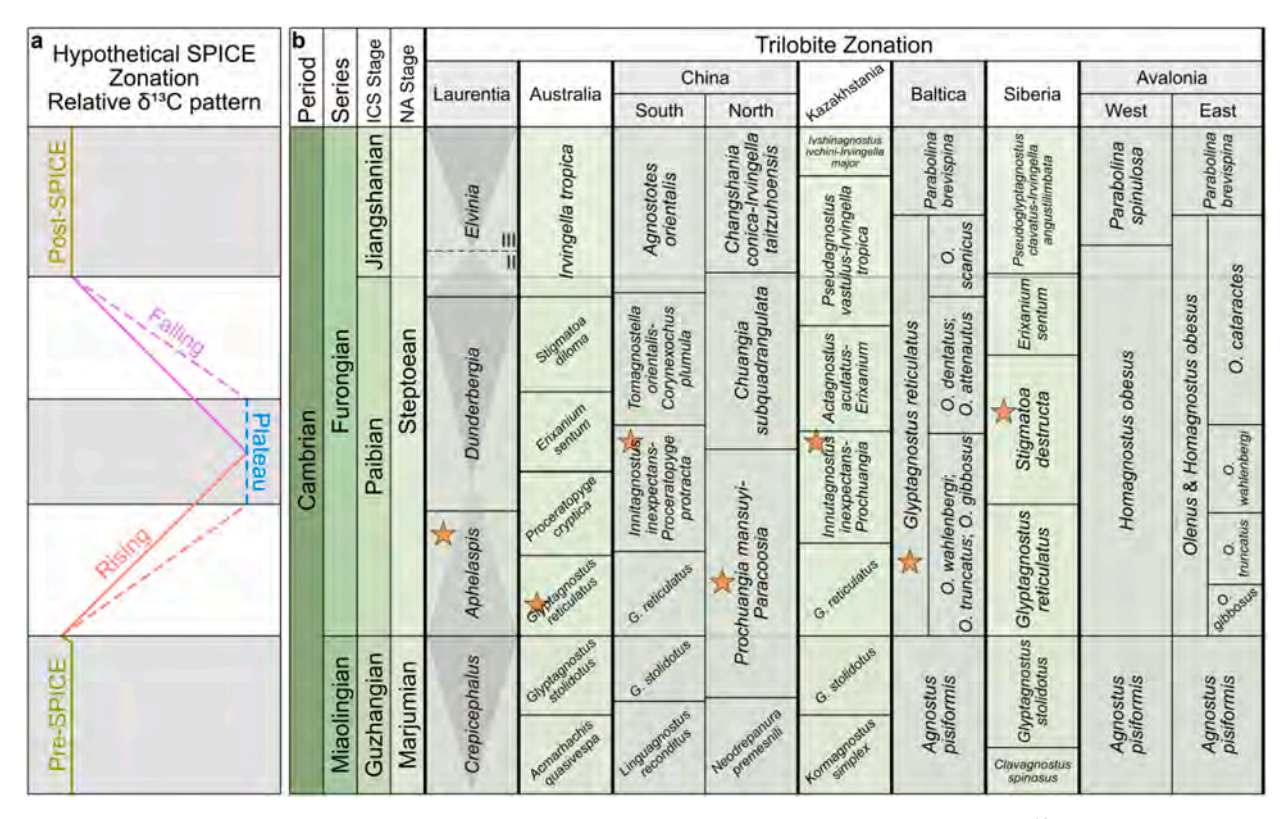


Fig. 1. Representative SPICE curve, Cambrian Series and Stage framework, and trilobite zonation correlation. (a) Idealized  $\delta^{13}$ C curve illustrating the 5 possible SPICE zones used to evaluate the stratigraphic expression of the SPICE (labeled, from lower to upper): Pre-SPICE, Rising limb, Plateau, Falling limb, and Post-SPICE. The zonation color-coding used here is also adopted in further figures. (b) Global correlation scheme of trilobite biozones, after Geyer (2019). Orange stars indicate the timing of the onset of the rising limb of the SPICE as identified on different paleocontinents (from Saltzman et al., 2000; Kouchinsky et al., 2008; Ahlberg et al., 2009; Ng et al., 2014; Schmid et al., 2018; and Pruss et al., 2019, as noted by Geyer, 2019). The transgressive and regressive packages within the Sauk II and Sauk III megasequences (after Palmer et al., 2012) are indicated by the triangle diagrams overprinted on the Laurentian trilobite zones; the Sauk III-Sauk III boundary is indicated by the dashed line in the Laurentia column. Note that (a) and (b) are not intended to directly correlate, their positions are only relative.

2011; Schiffbauer et al., 2017).  $\delta^{13}$ C values rise toward a maximum of approximately +4 to +5% in the late *Dunderbergia* or early *Elvinia* zones, with the peak preceding the FAD of Irvingella major and coinciding with the Sauk II-Sauk III megasequence boundary (Sloss, 1963; Saltzman et al., 2000, 2004; Glumac, 2011; Wotte and Strauss, 2015). The return to background  $\delta^{13}$ C values occurs within the *Elvinia* zone and the latest Pterocephaliid biomere, preceding the Marjumiid-Pterocephaliid boundary and extinction event (Glumac, 2011; Wotte and Strauss, 2015; Saltzman et al., 2004). Much more broadly, the SPICE event occurred between the Cambrian radiation and the Great Ordovician Biodiversification Event (GOBE) and has been posited to reflect changes in paleoenvironmental conditions leading to either the GOBE or the Ordovician Plankton Revolution (Servais et al., 2016). Although no direct link has been established between the SPICE and these biotic events, the SPICE may record conditions that set the stage for development of the appropriate oxygenation and/or nutrient conditions for later biodiversification (Servais et al., 2008, 2016; Saltzman et al., 2011).

Several authors have documented the peak of the SPICE being coincident with the Sauk II-Sauk III megasequence boundary in Laurentian sections (Saltzman et al., 1998, 2004; Glumac and Mutti, 2007; Glumac, 2011). This necessitates deposition of strata recording the rising limb of the SPICE during the tail end of a regressive event, and subsequent deposition of strata capturing the falling limb during the beginning of a transgression. While the Sauk sequences specifically are directly applicable to Laurentian strata, some authors have suggested that sections elsewhere in the world may also record a shallowing event coincident with the SPICE (e.g., Chen et al., 2011; Wotte and Strauss, 2015; Wang et al., 2020), although this is not ubiquitous (e.g., Schiffbauer et al., 2017; LeRoy and Gill, 2019; Labotka and Freiburg, 2020). The SPICE is not the only carbon isotope excursion in the Paleozoic that is associated with eustatic sea-level changes. For instance, the positive Upper Ordovician Hirnantian isotopic carbon excursion (HICE) has been attributed to glacioeustacy (Melchin et al., 2013; Jones et al., 2020); and comparably, the positive  $\delta^{13}\text{C}$  excursion of the Silurian Ireviken event is suggested to have been linked to climate change (Rose et al., 2019). This latter excursion is sometimes recorded in regressive facies packages (Baltica and Canada), and sometimes in transgressive facies packages (USA, Great Britain, and Tunisia) (Rose et al., 2019), similar to what is observed for the SPICE.

Despite its reputed global nature, some workers have suggested that the SPICE event may be more strongly affected by regional/local depositional conditions than previously thought—and thus its utility for correlation may be imprecise. Some workers have cited regional tectonics, heterogeneity in the chemical gradients of seawater in the Furongian, and paleo-water depth as potential driving forces for this variability (Wotte and Strauss, 2015; Schiffbauer et al., 2017; Barili et al., 2018). Furthermore, the SPICE interval varies widely in stratigraphic thickness, from <3 m in the Wanliangyu section, China (Rising limb: ~1 m; Chen et al., 2011) to >800 m in the Kulyumbe section, Siberia (Rising limb: ~380 m; Kouchinsky et al., 2008). In addition to demonstrable local variability, some sections that have been previously identified as Steptoean in age do not capture an easily identifiable SPICE signal in their  $\delta^{13}$ C records, despite clear documentation of the event in nearby time-equivalent units (e.g., Pruss et al., 2016). The fossil assemblages in some of these sections indicate a likely Steptoean age (e.g., Huang et al., 2019), whereas in other sections, fossil data are sparse, causing ambiguity about the age of the units (e.g., Glumac and Mutti, 2007).

These disparities, among others later discussed, in published SPICE data make its use as a tool for global correlation more complicated than previously assumed. To date, no robust statistical analyses have been employed to quantitatively compare and contrast the stratigraphic expressions of the SPICE. Identification of the excursion has been done predominantly through C-isotope pattern-matching, for lack of a better term, and biostratigraphic and/or lithologic correlation. Here, we present a compilation of data from the published literature and the results

of a meta-analysis to test for emergent patterns in the  $\delta^{13} C$  records of the SPICE and explore a variety of regional/local conditions during deposition and diagenesis that may have impacted its stratigraphic expression.

## 2. Materials and methods

## 2.1. Construction of the SPICErag

To test the variability of the stratigraphic and isotopic expression of the SPICE signal, we compiled a database of SPICE records published from 1992 to 2020 (data collection was stopped on February 29, 2020). In sum, the entire compilation encompassed a total of 95 individual sections from 36 published journal articles and theses/dissertations—78 of which were subjected to statistical analyses (see Table 1 for summary), and 17 of which were excluded for their lack of an apparent excursion. Hereafter, we refer to this database as the Steptoean Positive Isotopic Carbon Excursion repository for quantitative analysis (the SPICEraq). Three publications prior to Saltzman et al. (1998), where the SPICE received its formal definition, were included in this study because they report data that tenably recorded the then-unnamed SPICE event: Laudon (1992), He (1995), and Saltzman et al. (1995). Carbon isotope data, and, if noted, lithology and/or facies, were taken from supplemental files and in-text tables provided for each published SPICE dataset. If not provided in tables, lithology and/or facies were extracted from the text and/or figures of the corresponding publication. Where necessitated by the lack of published data tables,  $\delta^{13}$ C values and stratigraphic thickness measurements were extracted from figures using WebPlot Digitizer (WPD; Rohatgi, 2019—all extracted data are included in the SPICEraq). In many cases, WPD was used for extracting metadata other than isotope values and stratigraphic heights/core depths, for instance including Series/Stage boundary positions, Formation boundary positions, lithologic package thicknesses, biostratigraphic index or biozone boundary positions, and other information included in figures but not reported in data tables (this information is explicitly provided in the Supplementary Online Materials [SOM], Appendix 1).

In order to quantitatively evaluate the expression of the SPICE event,  $\delta^{13}\text{C}$  curves were divided into 5 possible "SPICE zones" based on the shape of the curve and/or the greater stratigraphic context of the section as relayed in the text and figures of the corresponding papers (Fig. 1a). To be clear, while the excursion itself is commonly defined as a 4 to 5% shift in  $\delta^{13}$ C values, we chose not to demarcate the SPICE zones designated herein either by specific  $\delta^{13}$ C values or magnitudes of change. Instead, because marked variation is observable both across and within entries, we visually assessed all of the compiled data, scaled equally within groups organized by stratigraphic thickness. From our observations, we have defined the SPICE zones as follows, largely based on changes in the slope of the  $\delta^{13}$ C profile over stratigraphic distance: (1) Pre-SPICE: background  $\delta^{13}$ C values prior to the onset of the SPICE. (2) Rising limb: the onset of the SPICE, beginning with the negative-most value immediately preceding the rise in  $\delta^{13}C$  and ending with the maximum  $\delta^{13}C$  value prior to a plateau or fall. (3) Plateau: for those sections that hovered near the peak  $\delta^{13}C$  value for a minimum of 5 m, a plateau was demarcated between the maxima of the rising and falling limbs. (4) Falling limb: the zone over which  $\delta^{13}$ C values return to a stabilized background, beginning with the maximum  $\delta^{13}$ C value or the end of the rising limb/plateau, and ending with the negative-most  $\delta^{13}$ C value before stabilization. (5) Post-SPICE: stabilized background  $\delta^{13}$ C values following termination of the falling limb (Fig. 1a). In order to preserve the full stratigraphic extent of each SPICE zone in subsequent analyses, the sample marking the boundary between adjacent SPICE zones was included in both the preceding and succeeding zones.

In several sections, the pre- and/or post-SPICE zones covered tens to hundreds of meters, capturing other excursions/fluctuations either before or after the SPICE. These zones were truncated in an attempt to remove these fluctuations and calculate median  $\delta^{13} C$  values that more

accurately reflect the baselines immediately under- and overlying the SPICE. The samples excluded from this study remain in the SPICEraq but have been coded as "Omit" for the SPICE zone. A corrected meters-above-the-bottom value was calculated for each section, with the 1st non-omitted sample used as the bottom-most value. However, to mitigate variation in stratigraphic thickness across datasets and to pin sections on an identifiable chemostratigraphic feature, the stratigraphic height or borehole depth of each sample was recalculated as meters relative to the onset of the rising limb of the SPICE event.

Five grouping variables were used to test for emerging patterns in the SPICEraq: paleolatitude, paleocontinent, water depth, facies, and lithology. Approximate paleolatitude and paleocontinent for each study locality were determined based on the 500 Ma paleogeographic reconstruction in GPlates (Müller et al., 2018). Six paleolatitudinal categories, as approximations of climate zones, were demarcated in 30° increments symmetrically about the equator (0-30°N and S; 30-60°N and S; and 60-90°N and S). The precise location of Kazakhstanian sections is not known at 500 Ma; following Saltzman et al. (2000), those sections are assumed to have been located between 0 and 30°S because the island arc that would later become Kazakhstania spans from the lower portion of 0-30°N zone to the upper portion of the 30-60°S zone (Fig. 2). Facies characterization for each section was simplified to one of five categories based on the description provided in the text for the onset of the SPICE: (1) Shallow/nearshore, (2) Shelf, (3) Intrashelf basin, (4) Slope, and (5) Basin. Water depth was approximated from these simplified facies categories, with 1 corresponding to shallow, 2 and 3 corresponding to intermediate, and 4 and 5 corresponding to deep. Table S1 lists the facies/ depth descriptors that served as keywords for our categorical assignment; such an approach was necessary because not all of the publications assessed for the SPICEraq database provide an approximate water depth for the deposition of the analyzed carbonates. Water depth thus operates as a more relaxed approximation of depositional environment than the facies descriptor. In order to evaluate the effects of lithology on  $\delta^{13}$ C values, the lithology of the sample recording the peak  $\delta^{13}$ C value for the rising limb of the SPICE was noted and simplified to one of three categories: (1) "Carbonate", (2) Limestone, and (3) Dolostone (n = 77

total). Samples included in the "carbonates" category represent those for which a more precise lithology (i.e., limestone or dolostone) could not be ascertained from data tables, stratigraphic columns, or the text of the original publications. Within individual entries, lithologies were not assessed for all samples nor were the effects of lithology on  $\delta^{13} C$  values evaluated for the entire SPICE interval because several entries comprise data obtained from both limestones and dolostones and thus cannot be assigned to a single lithologic category. Note that entry #49 was excluded from lithologic analysis because samples within this entry comprise only the falling limb of the SPICE.

Some of the sections included in our compilation, although identified as Steptoean in age, do not illustrate the characteristic positive  $\delta^{13}C$  excursion (n=17; including some or all sections from Perfetta et al., 1999; Glumac and Spivak-Birndorf, 2002; Buggisch et al., 2003; Glumac and Mutti, 2007; Sial et al., 2008; Ahlberg et al., 2009; Peng et al., 2016; Pruss et al., 2016; Jeffrey, 2017; Azmy, 2019; Huang et al., 2019). As a result, these sections cannot be broken down into the five "SPICE zones" used in this study to describe the excursion and have thus been excluded from further analysis of the SPICEraq. This group of sections is hereafter referred to as the "SWEETS" group (sections without evident expression of the SPICE) because of their apparent lack of "SPICE-y-ness". Some of the sections in the SWEETS group may show portions of the SPICE, for instance a part of the rising or falling limbs. However, not enough detail is reported to confirm that they unequivocally capture the SPICE event or to justify their inclusion in further analyses.

Two publications that do unambiguously present SPICE-bearing sections were unfortunately necessary to exclude from both the SPICE-raq and the SWEETS group. The first is Brasier's (1993) seminal composite carbon isotope curve from the Great Basin, which is commonly regarded as the first documentation of the SPICE event (Saltzman et al., 2004; Barili et al., 2018). These data could not be evaluated because: (1) no data tables are provided in text; and (2) the isotope versus stratigraphy illustration (his Fig. 1) has no vertical scale. The second exclusion was Li et al. (2018a), which captures the SPICE event in a suite of well logs from south China. However, much like the other exclusion, these data are inaccessible because: (1) no data tables are provided; and (2)

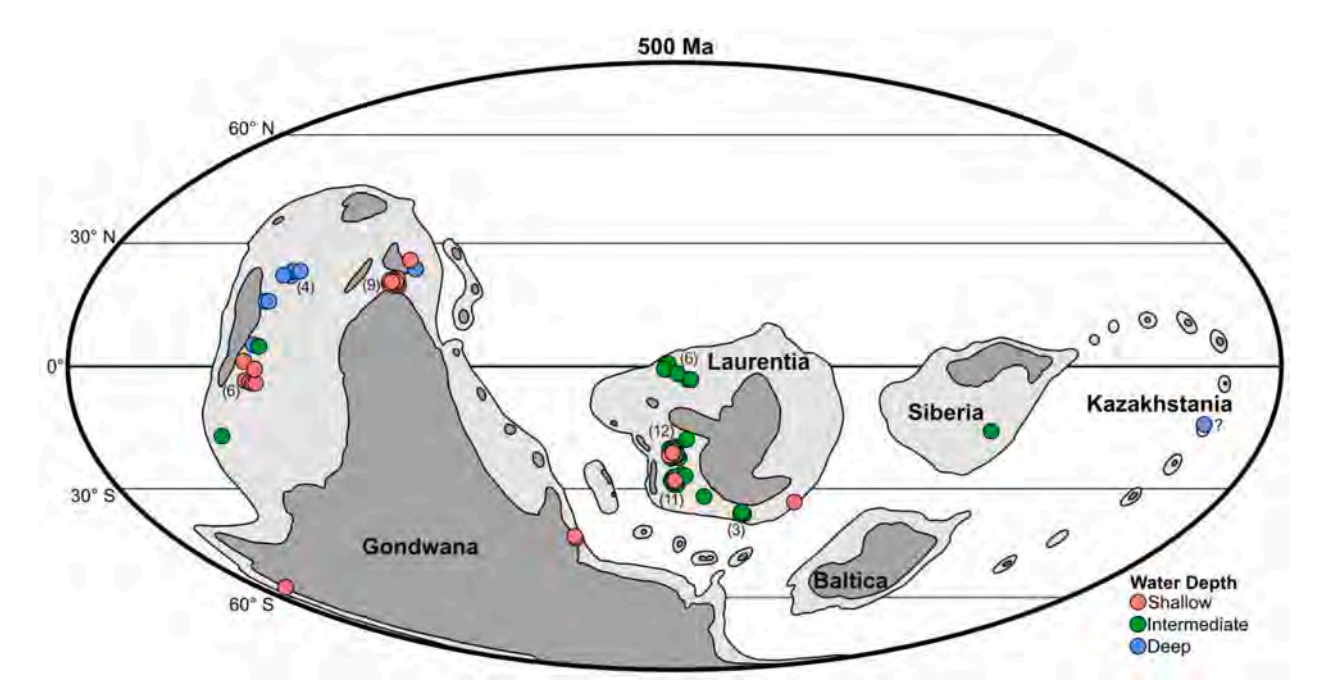


Fig. 2. Paleogeographic map ca. 500 Ma. The location of each of the 78 entries included in the SPICEraq is marked by a circle, color-coded by categorical water depth. The numbers in parentheses denote how many total entries are included within each overlapping cluster. A question mark denotes an uncertain paleogeographic location. Dark grey regions denote exposed continental land masses, whereas light grey regions denote continental shelves. Reconstruction based on the 500 Ma raster from GPlates (Müller et al., 2018). (For interpretation of the references to color in this figure legend, the reader is referred to the web version of this article.)

the figures show only lines instead of individual data points that could have been assessed via WPD (and arbitrarily picking any "points" along the published curves may capture "smoothed" or otherwise filtered data).

The full SPICEraq database is included as a Microsoft® Excel® file in the SOM, with associated metadata in appendix 1 and a column key for the SPICEraq datasheet in appendix 7 within the SOM text file. In addition, metadata descriptions for the SWEETS group are included in

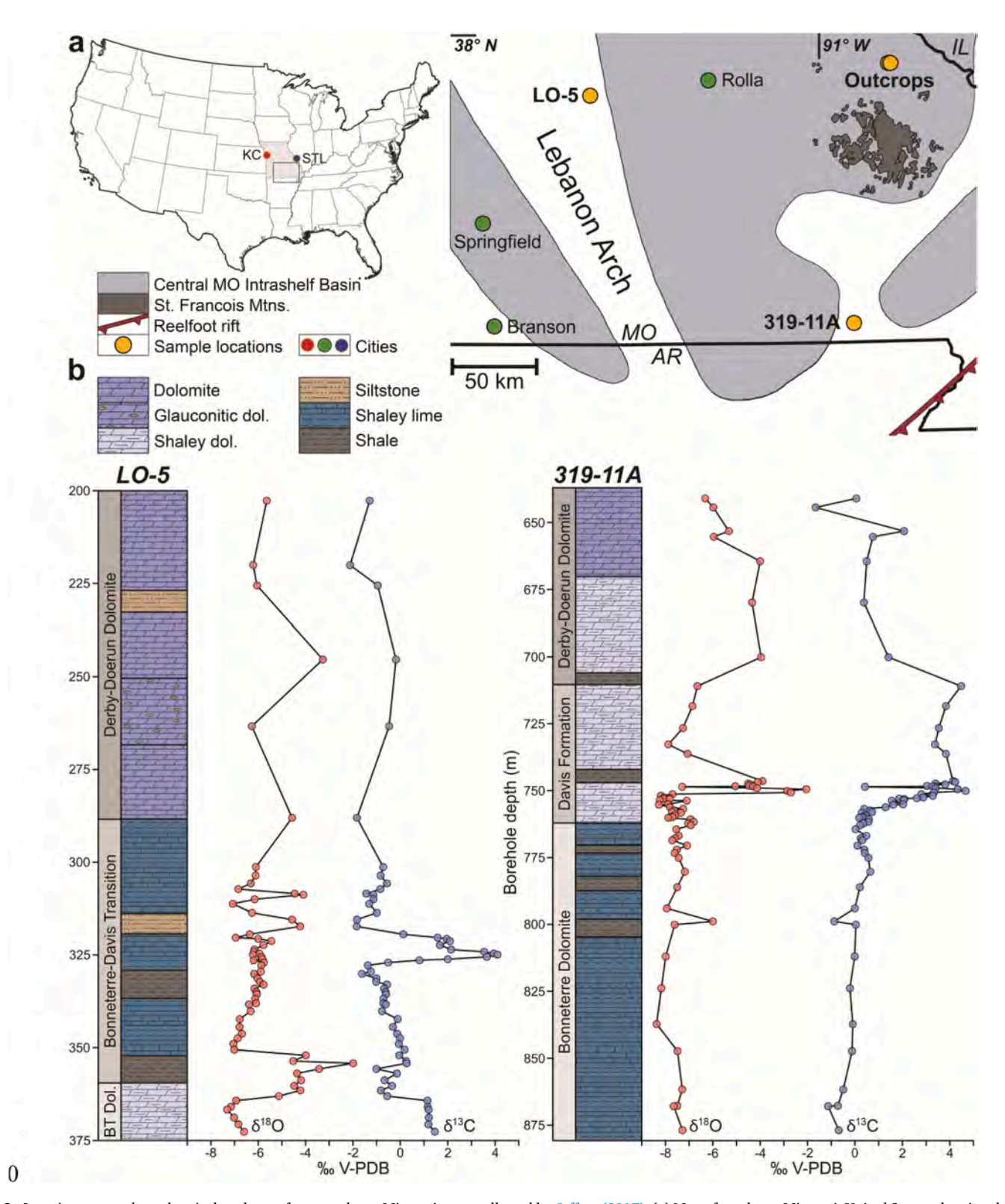


Fig. 3. Location map and geochemical analyses of two southeast Missouri cores collected by Jeffrey (2017). (a) Map of southeast Missouri, United States, showing the locations (yellow circles) of cores LO-5 and 319-11A, as well as sampled outcrops (data shown in Fig. S2), relative to the central Missouri Intrashelf Basin, Lebanon Arch, and Reelfoot Rift. (b) Lithologic core logs and geochemical analyses of LO-5 and 319-11A. Note that while the % V-PDB scales on the x-axes are identical, the vertical scales are different.

appendix 2 of the SOM text; paleogeographic locations of the SWEETS sections are included in Fig. S1; and all SWEETS  $\delta^{13}C$  data are plotted in Fig. S2. Where discussing any SPICEraq or SWEETS entries in the main text that follows, we include the entry numbers (corresponding to the database in #X format for SPICEraq entries and #SX format for SWEETS entries), along with their corresponding locations and references at their first in-text mention. Lastly, appendix 3 of the SOM text includes additional details on WPD data collection, as well as verification of the accuracy and precision of WPD through cross-checking of published sections with both figures and data tables available (examples shown in Fig. S3).

## 2.2. Quantitative analysis of the SPICEraq

RStudio (v. 1.2.1335 © 2009-2019 RStudio, Inc.) packages base and stats (v. 3.6.1; R Core Team, 2019) were used to identify the following δ<sup>13</sup>C values: pre-SPICE median, rising limb minimum, rising limb maximum, plateau median, falling limb minimum, and post-SPICE median. The ranges of both stratigraphic thicknesses and  $\delta^{13}$ C values for the SPICE zones were also calculated. Data wrangling and transformation in RStudio was accomplished with the dplyr (v. 0.8.3; Wickham et al., 2019) and tidyr (v. 0.8.3; Wickham and Henry, 2019) packages, Wilcoxon rank-sum tests were conducted using the stats package (v. 3.6.1; R Core Team, 2019) to compare pre-SPICE medians, rising limb minima, rising limb maxima, and post-SPICE medians among the identified grouping variables: paleolatitude, paleocontinent, water depth, facies, and lithology. This tests the alternative hypothesis that the data come from populations with the same median values. The statistical significance of differences in peak  $\delta^{13}$ C values across paleolatitudinal bins was further evaluated through randomization, the details of which are provided in the SOM (Appendix 4). In addition,  $\chi^2$  tests were conducted in PAST (v. 4.0; Hammer et al., 2001) in order to determine whether or not the presence of a plateau in SPICE data was related to paleolatitude, paleocontinent, water depth, or facies. The null hypothesis for the  $\chi^2$ tests is that the proportion of plateaus among grouping variables is indistinguishable from the proportion of all observations among those same grouping variables (i.e., the likelihood of a plateau is unaffected by grouping variable). An alpha value of 0.05 was assumed for all analyses, with marginally significant *p*-values constrained to 0.05 . Theggplot2 (v. 3.2.1; Wickham, 2016) and ggridges (v. 0.5.1; Wilke, 2018) packages in RStudio were used to produce figures. See SOM (Appendix 6) for a copy of our R code inputs.

## 2.3. Additional data from Southeast Missouri

In addition to previously published data, detailed samples for isotope analysis were collected from two cores from southeast Missouri, housed at the Missouri Geological Survey McCracken Core Library and Research Center in Rolla, MO (Jeffrey et al., 2017). These cores augment data reported by Schiffbauer et al. (2017) for the Central Missouri Intrashelf Basin. Core LO-5 represents a shallow marine section deposited on the Lebanon Arch, and core 319-11A represents a shelf section deposited on a down-dropping, fault-bounded block adjacent to the Reelfoot Rift (Fig. 3a; entries #38 and #39, respectively). Samples were sawn and examined via binocular microscopy to identify their lithological and mineralogical components. Carbonate portions were micro-drilled; care was taken to target homogeneous carbonate components, including micritic and oolitic calcite, and micritic, planar, and fabric-retentive dolomite (Sibley and Gregg, 1987). In addition, two southeast Missouri outcrops taken from the Jeffrey (2017) thesis are also reported for completeness, although they do not unequivocally record the SPICE and are thus placed in the SWEETS group. See the SOM (Appendix 2) for a further description of these outcrops and the corresponding  $\delta^{13}\text{C}$  and  $\delta^{18}$ O data (entries #S9 and #S10).

Analyses of carbon and oxygen isotopes were conducted at Washington University in St. Louis, MO, using a GasBench II peripheral on a

Delta V Advantage isotope ratio mass spectrometer (IRMS). Isotopic results are reported on the V-PDB scale; NBS 19 was used as the house standard, with replicate analyses giving a standard error of  $<\pm 0.05\%$  for both carbon and oxygen values.

## 3. Results

# 3.1. New $\delta^{13}$ C and $\delta^{18}$ O data from Southeast Missouri

Previously unpublished core data from southeast Missouri, cores LO5 and 319-11A, are included in the SPICEraq as entries #38 and #39. Biostratigraphic control is lacking for both cores in the original drilling reports, so correlation is limited to  $\delta^{13}C$  data and lithostratigraphy (Jeffrey, 2017; He et al., 1997). The LO-5 section is 169.93 m in length and comprises 67 analyzed samples. This section spans the upper Bonneterre Dolomite, the mixed carbonate-siliciclastic Bonneterre-Davis transition, and the lower Derby-Doerun Dolomite (Fig. 3b). The Davis Formation is not easily distinguishable in this shallow-water section. The SPICE event is recorded in a silty limestone interval near the middle of the Bonneterre-Davis transition as an  $\sim\!5.5\%$  positive shift in  $\delta^{13}C$  values over a thickness of  $\sim\!3$  m, with a peak  $\delta^{13}C$  value of +4.1%. No correlative excursion is exhibited in the  $\delta^{18}O$  data over the same interval.

The 319-11A section contains 72 samples, covers an interval of 235.92 m, and spans the Bonneterre Dolomite, the Davis Formation, and the lower Derby-Doerun Dolomite (Fig. 3b). In this section, the rising limb of the SPICE begins in the uppermost Bonneterre Dolomite and continues through the Davis Formation into the lowermost Derby-Doerun Dolomite. The magnitude of the positive  $\delta^{13}C$  shift is  $\sim\!5.0\%$ , and spans a stratigraphic interval of  $\sim\!6.5$  m, with a peak  $\delta^{13}C$  value of +4.67%. An  $\sim\!5.0\%$  positive shift in  $\delta^{18}O$  values correlates with the uppermost rising limb of the SPICE.

# 3.2. Results of the SPICEraq

Of the 95 sections assessed for compilation of the SPICEraq database, a total of 78 SPICE occurrences, comprising 6669 individual  $\delta^{13}$ C analyses, were included in the statistical evaluation presented here (Table 1; Figs. 4-7; SOM Appendix 1). The remaining 17 sections comprise the SWEETS group (Figs. S1-S2, SOM Appendix 2), which as described previously do not unequivocally show the excursion and are thus excluded from all results presented herein. Individual occurrences of stratigraphic sections/cores are referred to hereafter by their entry number in the SPICEraq (Table 1; Figs. 4-7; SOM). To avoid unnecessary repetition of lengthy figure captions, please refer to Table 2 for details pertaining to Figs. 4-7. These entries are from 40 unique stratigraphic sections and 25 unique drill cores, 12 of which have been sampled by more than one study. Importantly, sections with repeated analyses from more than one study were included in evaluation of the SPICEraq because they presented additional, rather than repeated, data. The following sections are represented by more than one entry in the SPICEraq: Felix Cove, Canada (entries #3 [Barili et al., 2018] and #30 [Saltzman et al., 2004]); House Range, United States (entries #2 [Baker, 2010], #24 [Saltzman et al., 1995], and #28 [Saltzman et al., 1998]); Shingle Pass, United States (entries #1 [Baker, 2010] and #27 [Saltzman et al., 1998]); TE-1 core, United States (entries #9 [Gill et al., 2011] and #37 [Schiffbauer et al., 2017]); Duibian A, China (entries #48 [Li et al., 2018b] and #64 [Zuo et al., 2018]); Kulyumbe, Siberia (entries #46 and #47 [Kouchinsky et al., 2008]); Kyrshabakty, Kazakhstan (entries #56 [Saltzman et al., 2000] and #61 [Wotte and Strauss, 2015]); Wa'ergang, China (entries #50 [Li et al., 2018b] and #55 [Saltzman et al., 2000]); Wangcun, China (entries #63 [Zhu et al., 2004] and #65 [Zuo et al., 2018]); Wanliangyu, China (entries #44 [Chen et al., 2011] and #60 [Wang et al., 2020]); Alice 1 core, Australia (entries #69 [Schmid, 2017] and #71 [Schmid et al., 2018]); and East Johnny's Creek 1 core, Australia (entries #70 [Schmid, 2017] and #75

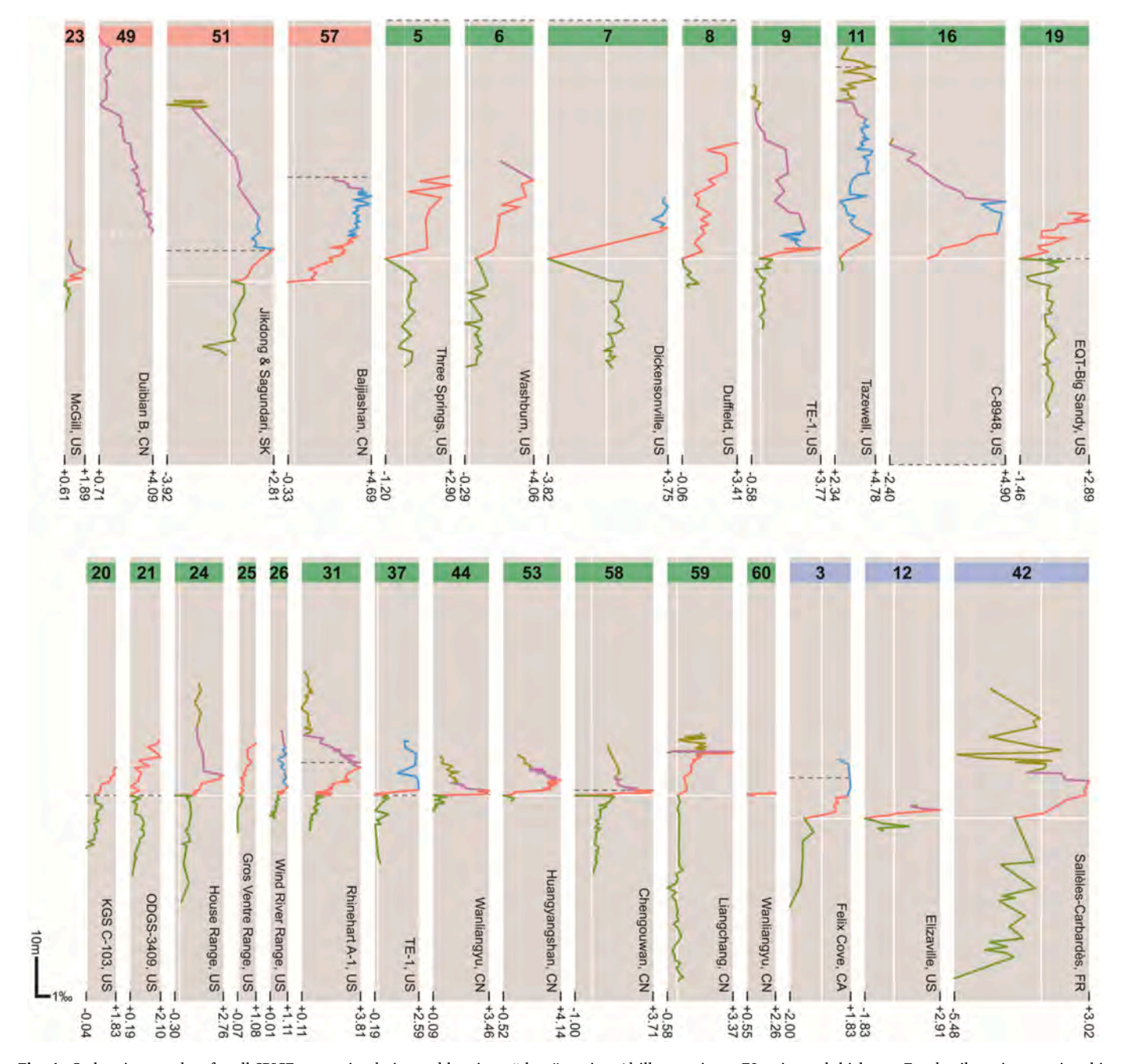


Fig. 4. Carbon isotope data for all SPICEraq entries designated herein as "short" sections/drill cores, i.e., <70 m in total thickness. For details on interpreting this figure, see Table 2.

## [Schmid et al., 2018]).

All studied sections were located between paleolatitudes of  $30^{\circ}$ N and  $60^{\circ}$ S, ca. 500 Ma, with the majority located from 0 to  $30^{\circ}$ S. Collection sites are located in 10 modern countries, sorted by number of included localities: United States (n=35), China (n=16), Australia (n=13), Canada (n=4), Kazakhstan (n=2), Siberia (n=2), South Korea (n=2), Argentina (n=2), France (n=1), and Scotland (n=1). These localities represent four paleocontinents—Gondwana, Kazakhstania, Laurentia, and Siberia—although all but four of the sections were located on either Laurentia or Gondwana. Shallow/nearshore (n=28) and intrashelf basin (n=21) facies are the most abundant categories, although the majority of these sections are from intermediate water depths (n=37). Deeper-water environments are represented mostly by slope facies (n=10), with rarer basin facies (n=3) (Table 3).

# 3.2.1. General $\delta^{13}C$ data summary

The  $\delta^{13}$ C values, stratigraphic thicknesses, and regional/local conditions of each entry are summarized in Table 1. The background median  $\delta^{13}$ C values prior to the onset of the SPICE range from -2.29 to +2.69% (entries #52 [Yaerdang Mountain, China; Liu et al., 2017] and #11 [Tazewell, Tennessee, US; Glumac, 2011], respectively). The maximum values of the rising limb, and thus the peak  $\delta^{13}$ C value of the SPICE event, range from +0.35 to +5.87% (entries #76 [East Mereenie 4, Australia; Schmid et al., 2018] and #68 [Mt. Whelan, Australia; Saltzman et al., 2000], respectively). The magnitude of the excursion ranges from 0.64 to 8.03% (entries #26 [Wind River Range, Wyoming, US; Saltzman et al., 1995] and #47 [Kulyumbe, Russia; Kouchinsky et al., 2008], respectively). After the peak,  $\delta^{13}$ C returns to lower values, stabilizing at a median post-SPICE background between -2.30 and +3.95% (entries #16 [C-8948, Illinois, US; Labotka and Freiburg, 2020]

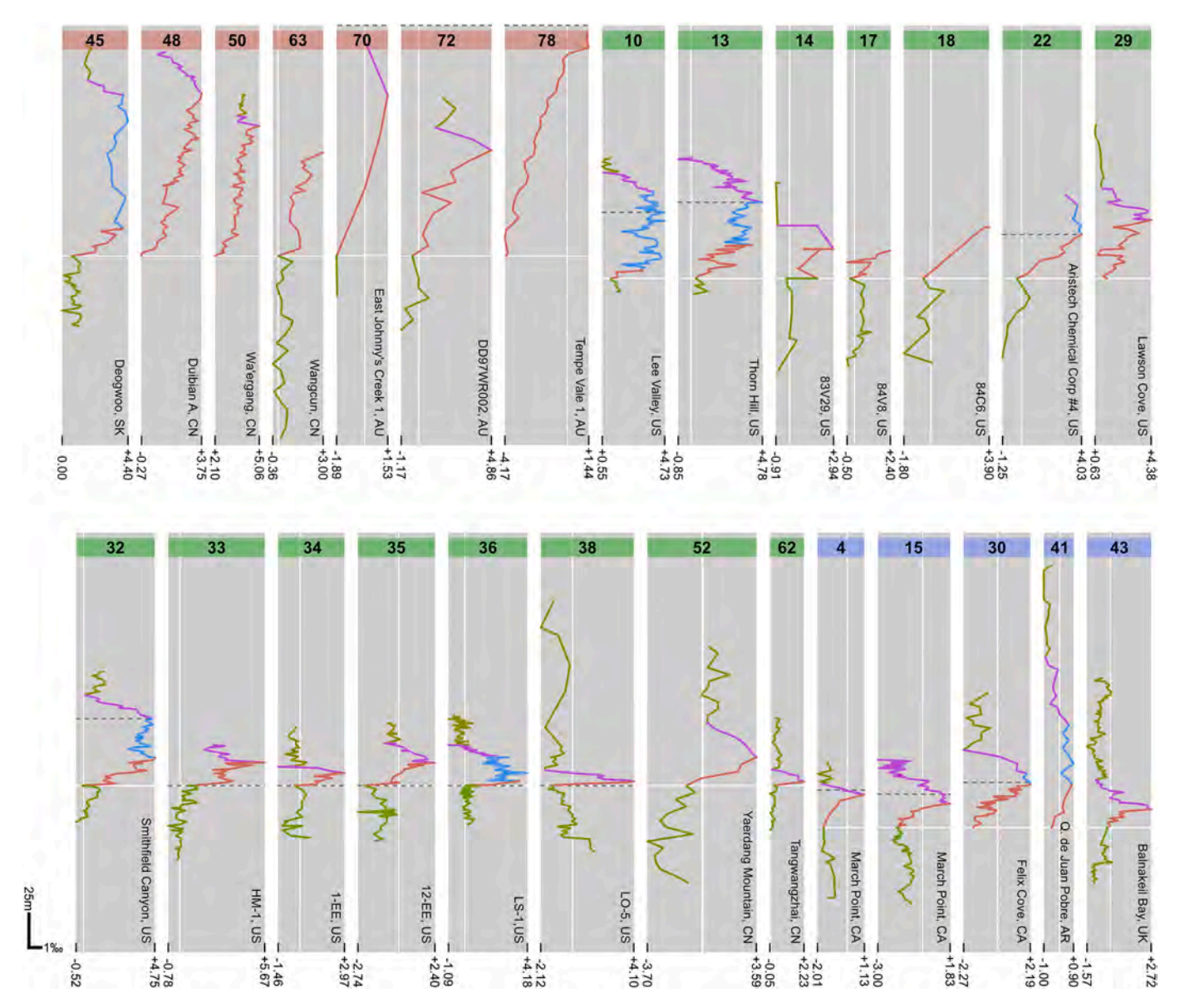


Fig. 5. Carbon isotope data for all SPICEraq entries designated herein as "intermediate" sections/drill cores, i.e., ≥70 and <200 m in total thickness. For details on interpreting this figure, see Table 2.

and #50 [Wa'ergang, China; Li et al., 2018b], respectively).

# 3.2.2. Stratigraphic thickness

The stratigraphic thickness of SPICE zones varies widely. Rising limb zones are between <1 and 378 m thick (entries #60 [Wanliangyu, China; Wang et al., 2020] and #46 [Kulyumbe, Russia; Kouchinsky et al., 2008], respectively) and falling limb zones are between <1 and 506 m thick (entries #59 [Liangchang, China; Wang et al., 2020] and #46, respectively). If present, the plateau can be up to 110 m thick (entry #55 [Wa'ergang, China; Saltzman et al., 2000]). The stratigraphic thickness of the entire SPICE interval (Rising limb + Plateau + Falling limb) ranges from 2.85 m (entry #44 [Wanliangyu, China; Chen et al., 2011]) to 884 m (entry #46 [Kulyumbe, Russia; Kouchinsky et al., 2008]).

Scatter plots (Figs. 8, S4) show stratigraphic thicknesses relative to the peak magnitude of the SPICE event in an attempt to visualize sediment accumulation by the various groupings. These types of data visualizations are organized by thickness of only the rising limb (Fig. 8) and then also as the thickness of the full excursion (Fig. S4), in order to differentiate any potential stratigraphic biases from the presence or

absence of a plateau. While rising limb thickness does not necessarily correlate directly with overall excursion thickness at the entry level, many of the same overall trends are present when viewed by various groupings. That is, the groups with statistically significant differences (by Wilcoxon rank sum tests) in rising limb thicknesses are also the groups that have statistically significant differences in total SPICE interval thicknesses (Table S2).

When stratigraphic thickness data are grouped by paleolatitude (Figs. 8a, S4a; Table S2a), the points, minus three outliers (entries #40 [Quebrada de La Angostura, Argentina; Sial et al., 2008], #46, and #47), form two clusters of stratigraphically thinner sections located in the southern hemisphere (Laurentia), and thicker sections located in the northern hemisphere (Gondwana). That the Laurentian sections are thinner than those in Gondwana is statistically significant (Table S2b). The Kazakhstanian sections, limited to two in number (entries #56 and #61), plot within the cluster for 0–30°S for both total and rising limb thicknesses (Figs. 8a–b, S4a–b). The Siberian sections are outliers (entries #46 and #47), bearing the thickest rising limbs over all, and being the only sections with rising limbs thicker than 100 m to have been deposited in the southern hemisphere (Figs. 8a–b, S4a–b). Entry #46

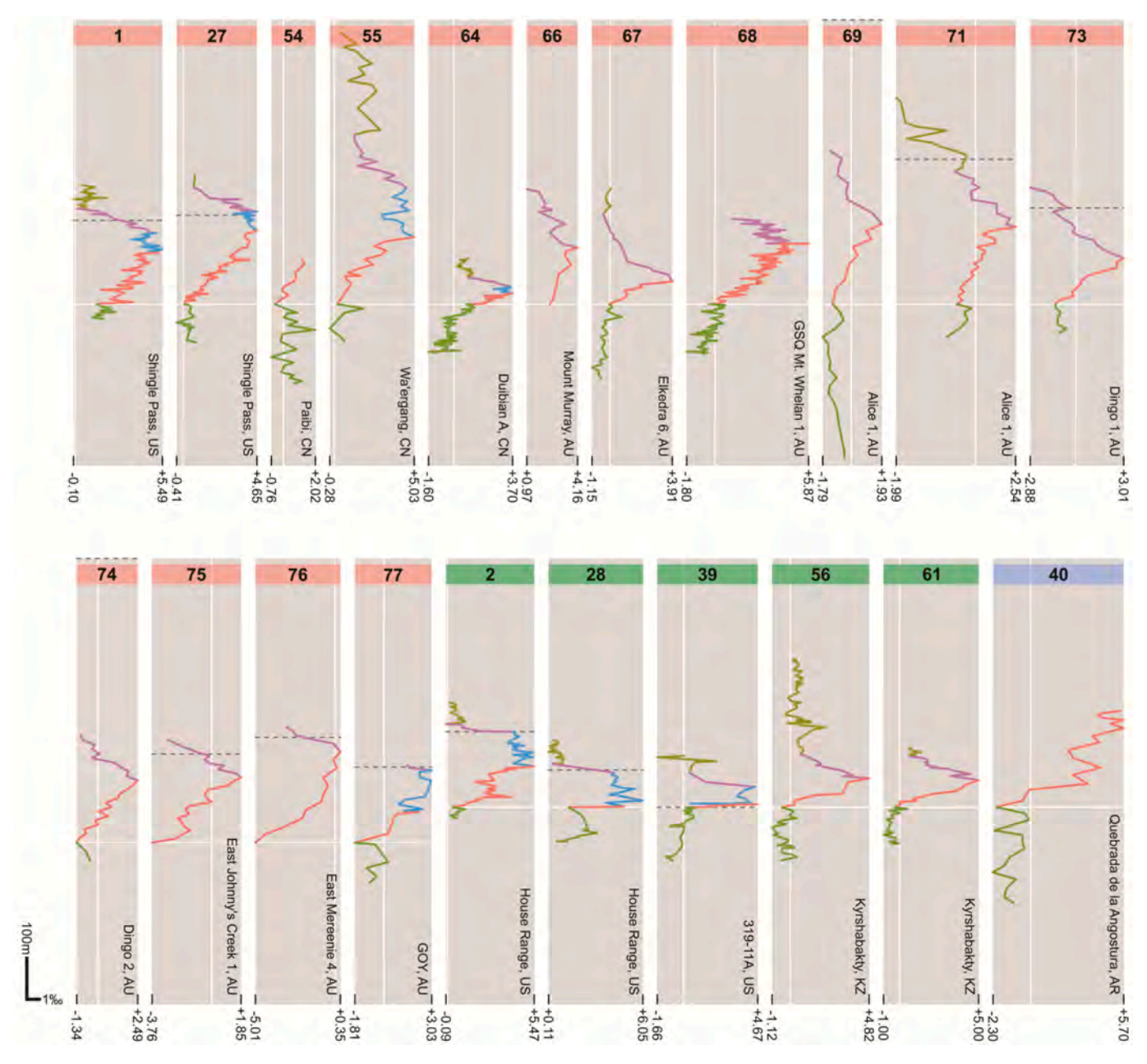


Fig. 6. Carbon isotope data for all SPICEraq entries designated herein as "long" sections/drill cores, i.e., ≥200 and <700 m in total thickness. For details on interpreting this figure, see Table 2.

also records the thickest total SPICE interval, which is at least 500 m greater than any other section (Fig. S4b).

There is significant overlap between groups when the sections are classified by water depth or facies (Figs. 8c–d, S4c–d). Intermediate water depths and facies tend to have stratigraphically thin total SPICE intervals and rising limbs (Figs. 8c, S4c). With the exception of the two notable Siberian outliers (entries #46 and #47), shelf facies display the narrowest range of stratigraphic thicknesses, with total SPICE intervals <100 m thick and rising limbs <50 m thick (Figs. 8d, S4d). Similarly, the majority of sections from intrashelf basin facies also have rising limbs <50 m thick and total SPICE intervals <100 m thick, with the exception of three outliers (entries #1, #2 [Baker, 2010], and #27 [Saltzman et al., 1998], all of which were deposited in the House Range Embayment within the Great Basin region of Laurentia). All but one of the slope sections (#45 [Deogwoo, South Korea; Chung et al., 2011]) plot between 50 and 150 m of stratigraphic thickness in the rising limb. While sections from intermediate water depths and the corresponding facies

have significantly shorter rising limbs and total SPICE intervals than sections deposited in slope settings, no further patterns are otherwise apparent across depth and facies groupings (Table S2c-d).

Supplementing the patterns observable in the scatter plots, box and whisker plots shown in supplemental figs. S5 and S6 highlight the similarities in the distribution of total excursion and rising limb thicknesses, respectively, across the grouping variables. Visually, the patterns in the equivalent figure panels are nearly identical, although the precise positions of median values and interquartile ranges may have shifted. The box and whisker plots further illustrate that the broader groups with stratigraphically thin rising limbs also tend to have stratigraphically thin total SPICE intervals (Figs. S5 and S6).

# 3.2.3. Statistical evaluation of the presence of a plateau

Twenty-five of the 78 (32%) total sections exhibit a plateau in elevated  $\delta^{13}C$  values between the rising and falling limbs. We used  $\chi^2$  tests to evaluate the null hypothesis that there is no association between

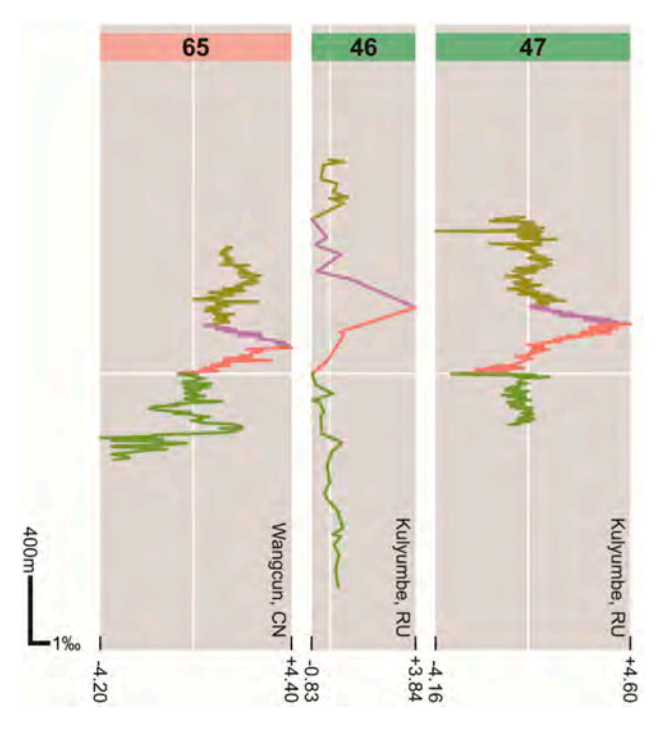


Fig. 7. Carbon isotope data for all SPICEraq entries designated herein as "super long" sections/drill cores, i.e.,  $\geq$ 700 m in total thickness. For details on interpreting this figure, see Table 2.

the presence of a plateau in individual SPICE entries and the grouping variables evaluated in this study. For all grouping variables, the resultant *p*-values for the  $\chi^2$  distributions are >0.1 (Table 4), and thus we failed to reject our null hypothesis.

# 3.2.4. Distribution and variation of SPICE zones and $\delta^{13}$ C values

Joy plots (or ridgeline plots/stacked density plots) illustrate changes in  $\delta^{13}$ C values through the progression of the SPICE across the categorical variables. In the case of paleolatitude, the sections in the 30–60°S zone have  $\delta^{13}$ C values approximately 1 to 2% lower than those from more equatorial regions (Fig. 9a). The differences between 30-60°S and 0-30°S sections are statistically significant in all cases, whereas the differences between 30-60°S and 0-30°N sections are only marginally significant for all cases except the maximum  $\delta^{13}C$  value of the SPICE (Table S3a).  $0-30^{\circ}N$  and  $0-30^{\circ}S$  sections have similar distributions; only the pre-SPICE median  $\delta^{13}$ C value is marginally significant (Fig. 9a; Table S3a). Randomization results indicate that the true difference in median peak  $\delta^{13} \text{C}$  values for higher latitude (30–60° S) sections relative to the combined median peak  $\delta^{13}$ C value of tropical (0–30° N and 0–30° S) sections is statistically significant (Fig. S7). Siberian and Kazakhstanian sections are omitted from the paleocontinent joy plot (Fig. 9b) because each has only two sections, rendering density plots impractical as tools for analysis or visualization. The overall shape of the distributions for Gondwanan and Laurentian sections are quite similar (Fig. 9b), except in the case of the pre-SPICE median  $\delta^{13}$ C values, in which Laurentian sections have a more pronounced peak about the median value, and a longer right tail. Fig. 9b confirms that the pre-SPICE median  $\delta^{13}$ C is significantly higher in Laurentia than in Gondwana; whereas the post-SPICE median  $\delta^{13}$ C is marginally higher in Gondwana than in Laurentia (Table S3b), as is described in more detail below in section 3.2.5. Most other differences in  $\delta^{13}C$  values between paleocontinents have no statistical significance (Table S3b).

Depth and facies joy plots show that, generally, the minimum and median  $\delta^{13}$ C values for the peak of the SPICE and the median of the post-SPICE background decrease with decreasing water depth (Fig. 10a). This trend is less obvious when sections are grouped according to facies

**Table 2**Key details for interpreting Figs. 4–7, S2.

Entries are grouped according to total length (in meters) of the section, excluding samples omitted from the pre- and post-SPICE zones for analytical purposes. Note that these groupings are for visualization purposes only, and do not reflect the stratigraphic thickness of the excursion itself, which can be found in Table 1:

- Short (x<70 m; Fig. 4)
- Intermediate (70≤x<200 m; Fig. 5)
- Long (200≤x<700 m; Fig. 6)
- Super long (x≥700 m; Fig. 7)
- Y-axis scale (stratigraphic thickness) is maintained within each figure (except in Fig. S2, where thickness groupings are labeled)

#### Within each plot:

- Section entry numbers, corresponding to the SPICEraq database, are noted at the top of each plot
- Section name/location is included at lower-end of each plot
- o Locations abbreviated as follows:
  - US = United States
  - CA = Canada
  - AR = Argentina
  - FR = France
  - SK = South Korea
  - CN = China
  - KZ = Kazakhstan
  - AU = Australia
  - RU = Russia
  - SE = Sweden (only used in Fig. S2)
- X-axis scale (δ<sup>13</sup>C ‰ V-PDB) is identical for all plots
- Grey boxes demarcate the range of 8<sup>13</sup>C values in each entry, with the minimum and maximum values denoted at the bottom of each plot
- Vertical white lines within the grey boxes indicate the position of 0‰ if it falls within the range of plotted values
- $\bullet$  Entries are aligned on the minimum  $\delta^{13}$ C value of the rising limb (the onset of the excursion), the position of which is denoted by the horizontal white line within the grey boxes
  - o Note that the position of entry #49 in Fig. 4 relative to others in this figure is only approximate; data from this section lie entirely within the falling limb
- The Sauk II–Sauk III boundary is denoted by a dashed horizontal line, dark grey in color, if its position relative to the plotted  $\delta^{13}$ C data was provided in the original publication (regardless of paleocontinent)

Sections are categorically grouped by paleolatitude, with color-coded entry number label flags to match paleolatitude groupings in other figures within both the main-text and SOM:

- $\bullet \ 0\text{--}30^{\circ}\ N=red$
- 0–30° S = green
- 30–60° S = blue

Carbon isotope data is color-coded according to SPICE zone, matching those used in Fig. 1a  $\,$ 

- Pre-SPICE = green
- Rising limb = red
- $\bullet \ \ Plateau \ [if \ present] = blue$
- $\bullet \ \ Falling \ Limb = purple$
- Post-SPICE = olive

(Fig. 10b) rather than water depth. For the pre-SPICE median and rising limb minimum, the higher  $\delta^{13}\text{C}$  values are found in intermediate depth (specifically intrashelf basin facies) sections, whereas shallow and deepwater sections have a nearly identical median value (Fig. 10; Table S3c). In contrast, the peak value of the SPICE excursion, and the median of the post-SPICE zone are highest in the deep-water (specifically slope facies) sections. (Fig. 10; Table S3d).

Box and whisker plots illustrate the magnitude of the  $\delta^{13}C$  excursion captured by the rising limb of the SPICE event (as the difference between the peak and onset  $\delta^{13}C$  values). The interquartile ranges and median values for the southern hemisphere are nearly identical, with no statistically significant differences (Fig. 11a; Table S3a). High magnitude  $\delta^{13}C$  excursions of  $\sim\!8\%$  are limited to sections from the southern hemisphere. Laurentian and Gondwanan sections have nearly identical interquartile ranges and similar overall ranges (Fig. 11b; Table S3b). Kazakhstanian and Siberian sections are included in Fig. 11b, although little can be said about their distributions relative to other paleocontinents due to conspicuously uneven sampling, except for the fact that both paleocontinents plot toward the higher end of the observed range. These high-magnitude  $\delta^{13}C$  excursions of  $\sim\!8\%$  are limited to shallow and intermediate depths, and thus shallow/nearshore, shelf,

Table 3

SPICE zone distributions. Distribution of entire entries, as well as individual SPICE zones across the categorical variables of interest to this study: paleolatitude, paleocontinent, water depth, facies, and lithology. Lithologic categories were not applied to entire SPICE zones.

Grouping variables	Grouping categories	Total entries (#)	Number o	f SPICE zones			
			Pre	Rising	Plateau	Falling	Post
Paleolatitude	0–30° N	27	19	26	8	24	12
	0–30° S	42	39	42	14	31	26
	30–60° S	9	7	9	3	7	6
Paleocontinent	Gondwana	34	24	33	7	29	17
	Kazakhstania	2	2	2	0	2	2
	Laurentia	40	37	40	18	29	23
	Siberia	2	2	2	0	2	2
Depth	Shallow	28	21	28	4	23	13
	Intermediate	37	34	37	18	28	23
	Deep	13	10	12	3	11	8
Facies	Shallow/nearshore	28	21	28	4	23	13
	Shelf	16	15	16	9	14	11
	Intrashelf basin	21	19	21	9	14	12
	Slope	10	7	9	2	8	6
	Basin	3	3	3	1	3	2
Total		78	65	77	25	62	44
Lithology	"Carbonate"	25	-	-	-	-	-
	Limestone	38	-	-	-	-	-
	Dolostone	14	-	-	-	-	-
	Total	77	_	-	_	-	_

and intrashelf basin facies (Fig. 11c–d). The interquartile range and median magnitude of shelf sections are both skewed more toward lower  $\delta^{13} C$  values than for any other facies (Fig. 11d). Slope and shelf settings have the widest interquartile ranges, whereas intrashelf basins have the narrowest range (Fig. 11d). For intermediate and deep-water facies, minimum and median  $\delta^{13} C$  magnitudes increase with water depth, with the highest minimum and median values found in basinal facies (Fig. 11c–d). Shallow/nearshore sections are exceptions to this trend, and are shifted more toward higher  $\delta^{13} C$  values relative to the sections deposited in shelf settings. (Fig. 11d). Note, however, that there are no statistically significant differences between these distributions of magnitudes (Table S3c–d).

# 3.2.5. Trends at the SPICE onset, and pre- to post-SPICE $\delta^{13}C$ shifts

In all cases, comparison of the  $\delta^{13}$ C value of the onset of the rising limb to the median  $\delta^{13}$ C value of the pre-SPICE zone in Figs. 9 and 10 shows a shift in the left tail of the distribution toward lower values. Forty-eight of the 78 total sections (62%) included in this database have minimum rising limb  $\delta^{13}$ C values that are lower than the median  $\delta^{13}$ C value of the pre-SPICE background. Twelve of the sections in the SPICEraq do not sample any of the pre-SPICE zone, which means that a median background  $\delta^{13}$ C value can only be calculated for 65 of the sections. Taking this into consideration, 74% of the sections with a recorded pre-SPICE zone display a small negative excursion immediately prior to the onset of the SPICE event (Perfetta et al., 1999). This "negative kick" has an average magnitude of 0.62%, and a maximum magnitude of 4.19% (Table 1). Depending on which grouping variable is used, the negative-most onset  $\delta^{13}$ C values of the SPICE are found in the 0-30°N zone, in Gondwana, and in shallow/nearshore settings (Figs. 9 and 10; Table S3). For further investigation of trends in rising limb, pre-, and post-SPICE data, see also data visualization in Figs. S8-S10.

# 3.2.6. Lithology

Fig. 12 illustrates the distribution of maximum rising limb  $\delta^{13}$ C values for those samples that could be identified as either limestone or dolostone. Samples limited to "carbonate" (n=25) for their lithologic description were excluded from this figure for visualization purposes. Results from the Wilcoxon rank sum tests are presented in Table S4. Limestone samples record marginally significantly higher peak-SPICE  $\delta^{13}$ C values (median = +3.76%; n=38) relative to dolostone samples (median = +2.69%; n=14).

#### 4. Discussion

## 4.1. Synopsis of the SPICE and potential causes

The SPICE is the most prominent positive carbon isotope excursion in the late Cambrian (Saltzman and Thomas, 2012). It has been hypothesized to be the result of such driving forces as: increased atmospheric oxygenation (Saltzman et al., 2011); higher rates of biological productivity (Saltzman et al., 1998, 2000); global cooling (Glumac and Walker, 1998; Saltzman et al., 1998); enhanced coastal upwelling (Saltzman et al., 2000); eustatic sea level change (Glumac and Walker, 1998; Saltzman et al., 2000, 2004); and an expansion of carbonate platforms (Álvaro et al., 2008). Most commonly, however, the SPICE event is attributed to: (1) an increased rate of burial of organic carbon (Glumac and Walker, 1998; Saltzman et al., 1998; Álvaro et al., 2008; Gill et al., 2011); (2) anoxic/euxinic conditions (Saltzman et al., 1998, 2000; Gill et al., 2011; Dahl et al., 2014; Bond and Grasby, 2017; LeRoy and Gill, 2019; Pruss et al., 2019); and/or (3) an increased rate of continental weathering associated with the sea level lowstand between the Sauk II and Sauk III megasequences (Glumac and Walker, 1998; Saltzman et al., 2000; Harper et al., 2019). In addition, anoxia and/or euxinia are commonly cited as the specific driver of the trilobite biomere turnover event associated with the SPICE, and it is therefore appealing to also assign this change in seawater chemistry as the source of the SPICE event itself. Documentation of correlative positive  $\delta^{34}\!S$  excursions in SPICE sections from the United States (Gill et al., 2007, 2011; Saltzman et al., 2011; LeRoy and Gill, 2019), Newfoundland (Hurtgen et al., 2009), Sweden (Gill et al., 2011), Kazakhstan (Wotte and Strauss, 2015), China (Saltzman et al., 2011), and Australia (Gill et al., 2011) may provide supporting evidence for anoxia and euxinia. Our methodology was specifically chosen in order to conduct a comprehensive analysis of the publication history of the SPICE event over the last 2+ decades and evaluate the potential significance of regional/local controls on the expression of the purportedly global signature of the SPICE in the rock record.

The SPICE is often depicted as an asymmetric excursion, with the rising limb noticeably thicker stratigraphically than the falling limb (see Fig. 1 in Glumac, 2011; Fig. 1 in Elrick et al., 2011; and Fig. 1 in Gerhardt and Gill, 2016), which does reflect the shapes of some SPICE excursions (e.g., entries #1, #4 [March Point, Canada; Barili et al., 2018], and #27). However, the stratigraphic expression of the SPICE is quite variable and does not typically display that geometry (Figs. 4–7). For

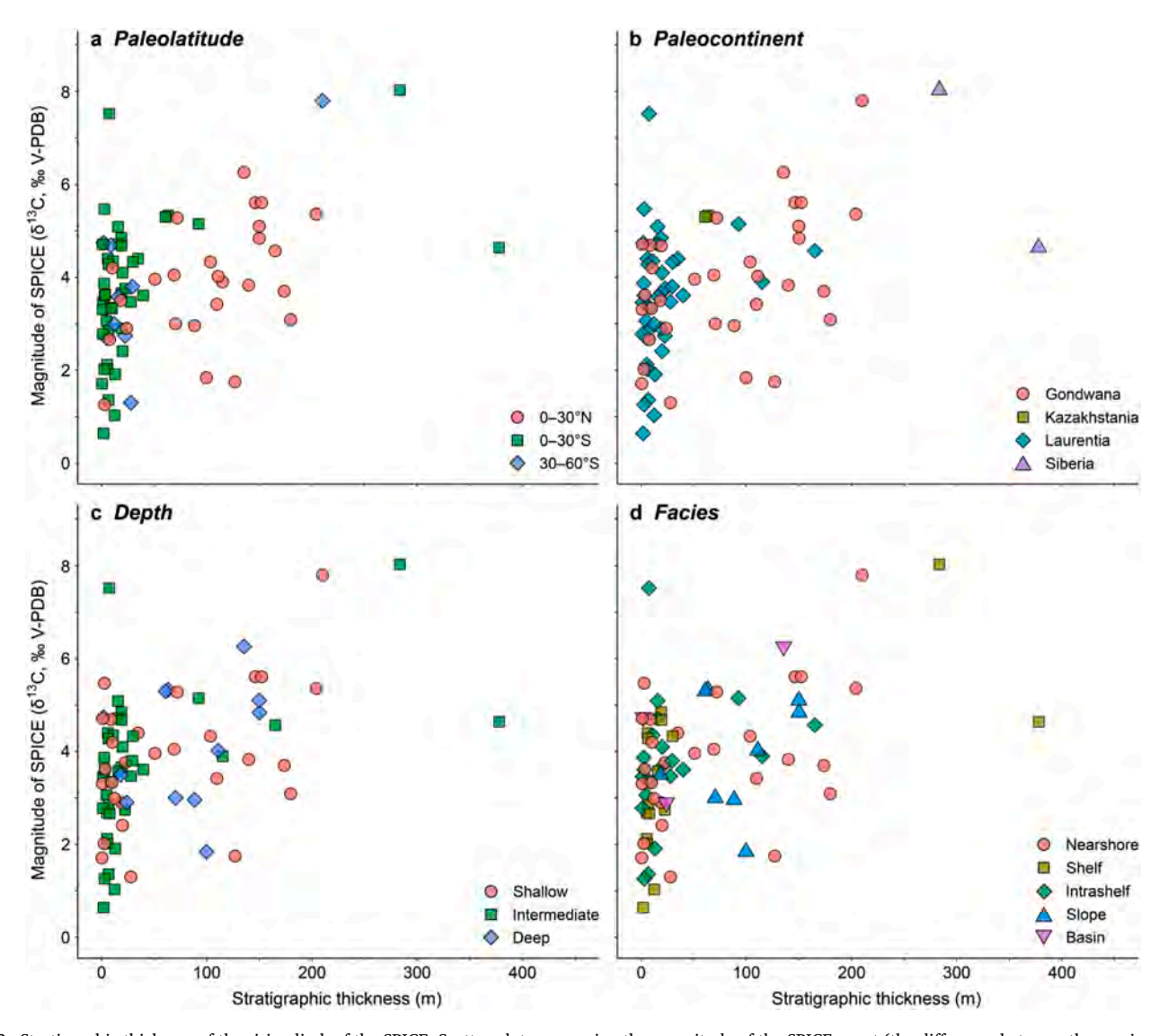


Fig. 8. Stratigraphic thickness of the rising limb of the SPICE. Scatter plots comparing the magnitude of the SPICE event (the difference between the maximum and minimum  $\delta^{13}$ C values of the rising limb) to the stratigraphic thickness (in meters) of the rising limb of the excursion. Together, these variables serve as a proxy for the rate of onset of the SPICE event. Entries are labeled according to the following grouping variables: (a) paleolatitudinal zone; (b) paleocontinent; (c) water-depth; (d) facies.

example, in some sections, the excursion is recorded as a sharp rising limb and much thicker falling limb (e.g., entries #9 [TE-1, United States; Gill et al., 2011] and #15 [March Point, Canada; Hurtgen et al., 2009]). Through the compilation conducted herein, however, we can observe that the SPICE has a more symmetrical appearance, with the rising and falling limbs covering comparable stratigraphic thicknesses (e.g., entries #31 [Rhinehart A-1, United States; Saltzman et al., 2004] and #32 [Smithfield Canyon, United States; Saltzman et al., 2004]). Perhaps more importantly, the SPICE interval varies widely in stratigraphic thickness, from <3 m in the Wanliangyu section, China (Chen et al., 2011) to >800 m in the Kulyumbe section, Siberia (Kouchinsky et al., 2008).

Our meta-analysis additionally demonstrates that the magnitude and peak values of the SPICE event are more variable than previously described. Following the classic account by Saltzman et al. (1998), the SPICE has typically been described as a positive  $\delta^{13} \text{C}$  shift,  $\sim\!4$  to 5% in magnitude. However, we illustrate through the SPICEraq data compilation that, in fact, the magnitudes of the excursion range from 0.64 to 8.03% (median = 3.76%), while the peak SPICE  $\delta^{13} \text{C}$  values range from +0.35 to +5.87% (median = +3.46%). This should not necessarily be unexpected, as the amount of research on SPICE-hosting sections has

increased dramatically since Saltzman et al.'s (1998) report—hence the motivation for this study. Despite the fact that the same general pattern can be seen in all sections that document the SPICE, the expression of the excursion in distinct sections appears fundamentally different in terms of the  $\delta^{13}$ C pattern and the stratigraphic thickness of the event. For example, see SPICEraq entries #9 (Missouri, US; Gill et al., 2011; short section with thin rising limb and plateau and a drawn-out falling limb), #45 (Deogwoo, South Korea; Chung et al., 2011; intermediate section with rising and falling limbs of similar thickness and a prolonged plateau), and #65 (Wangcun, China; Zuo et al., 2018; super-long section with relatively symmetric rising and falling limbs and no plateau; Figs. 4–7).

# 4.2. Interpretations of results

## 4.2.1. Plateaus

Although 32% of the entries included in the SPICEraq display a plateau, defined as persistently high  $\delta^{13}C$  values for 5 m or more of section (e.g., entry #28 [House Range, Utah, US; Saltzman et al., 1998]),  $\chi^2$  tests revealed that there is no significant association between the presence of a plateau in the SPICE record and any of the categorical

Table 4
Results for *Chi*-squared tests for the distribution of plateaus among grouping variables.

Grouping variables	Grouping categories	Plateau observed	Plateau expected	$\chi^2$ test results
Paleolatitude	0-30° N	8	8.15	$\chi^2 =$
				0.005
	0-30° S	14	13.92	df = 3
	30–60° S	3	2.93	p = 0.99
	Total	25	25	
Paleocontinent	Gondwana	7	10.07	$\chi^{2} = 2.24$
	Kazakhstania	0	0.73	df = 3
	Laurentia	18	13.46	p = 0.13
	Siberia	0	0.73	
	Total	25	25	
Depth	Shallow	4	8.15	$\chi^2 = 4.47$
	Intermediate	18	12.82	df = 2
	Deep	3	4.03	p = 0.11
	Total	25	25	
Facies	Shallow/ nearshore	4	8.15	$\chi^2 = 4.64$
	Shelf	9	5.95	df = 4
	Intrashelf basin	9	6.87	p = 0.33
	Slope	2	2.93	•
	Basin	1	1.10	
	Total	25	25	

variables investigated. Eighteen of the 25 plateau-bearing sections were deposited in intermediate water depths, indicating that shelf and intrashelf basin settings are the most likely to record a plateau, perhaps as a result of the combination of sediment supply and accommodation space (Schlager, 1993). However, 18 of 25 recorded plateaus are in sections from Laurentia, whereas the other 7 are in Gondwana, which may indicate higher sedimentation accumulation in Laurentia ca. 500 Ma. Contrary to this, the prevalence of stratigraphically thinner total excursions and rising limbs for Laurentian entries relative to those of Gondwana appears to suggest that, of the two paleocontinents, Laurentia may have been more sediment-starved during the onset of the SPICE (Figs. 8, S4). An alternative explanation to this phenomenon is that Laurentia may have been more tectonically quiescent than Gondwana at this time, and therefore would not have generated much new accommodation space, independent of sediment supply and delivery.

The uneven distribution of  $\delta^{13}C$  plateaus across Laurentia and Gondwana could be a product of the relationship between the SPICE event and the Sauk II-Sauk III transition. The peak of the SPICE has been described as correlating with the boundary between the Sauk II and Sauk III megasequences (Saltzman et al., 1998, 2004; Glumac and Mutti, 2007; Glumac, 2011). This would suggest that the rising limb of the SPICE was deposited during the tail end of a major regressive event, while the falling limb was deposited early during a transgression. However, Schiffbauer et al. (2017) suggested that the rising limb of the SPICE, at least in Missouri, United States, instead correlates with the early transgression of the Sauk III megasequence as evidenced by lithostratigraphic relationships in the studied cores. In those cores (entries #33-37), the rising limb of the SPICE is preserved in a package of deeper-water shales deposited atop shallow-shelf carbonates, which requires a deepening at or prior to the onset of the rising limb, rather than at the peak of the SPICE event as others have suggested (e.g., Brasier, 1993; Saltzman et al., 2004; Glumac, 2011). The SPICE in the Franconia Formation (entry #16; Labotka and Freiburg, 2020) of the regionally comparable Illinois Basin is preserved entirely within the Sauk III megasequence as also evidenced by stratigraphic relationships. Following a period of sea level fall prior to the onset of the SPICE, LeRoy and Gill (2019) additionally present evidence of sea level rise at the initiation of the positive excursion in the Conasauga Intrashelf Basin (entries #19-21; Appalachians), again in the form of deeper-water shales being deposited over shallower carbonate units. If, as Schiffbauer et al. (2017), Labotka and Freiburg (2020), and LeRoy and Gill

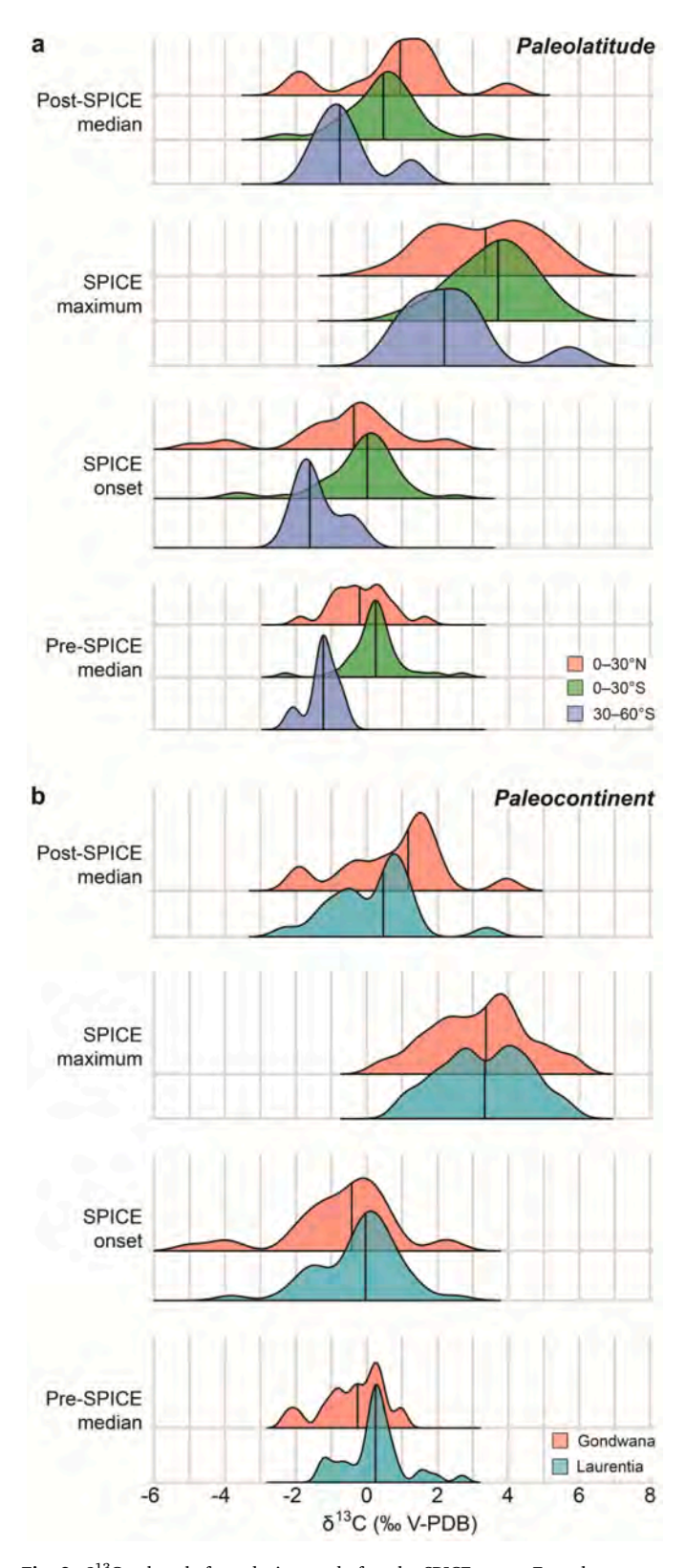


Fig. 9.  $\delta^{13}$ C values before, during, and after the SPICE event. From bottom to top the individual joy plot panels show the distribution in  $\delta^{13}$ C values for the median pre-SPICE background, the minimum of the rising limb (the onset of the SPICE event), the maximum of the rising limb (the peak of the SPICE event), and the median post-SPICE background. The vertical black line within each curve denotes the median value of that distribution. In (a), sections are grouped according to paleolatitude; in (b), sections are grouped according to paleocontinent.

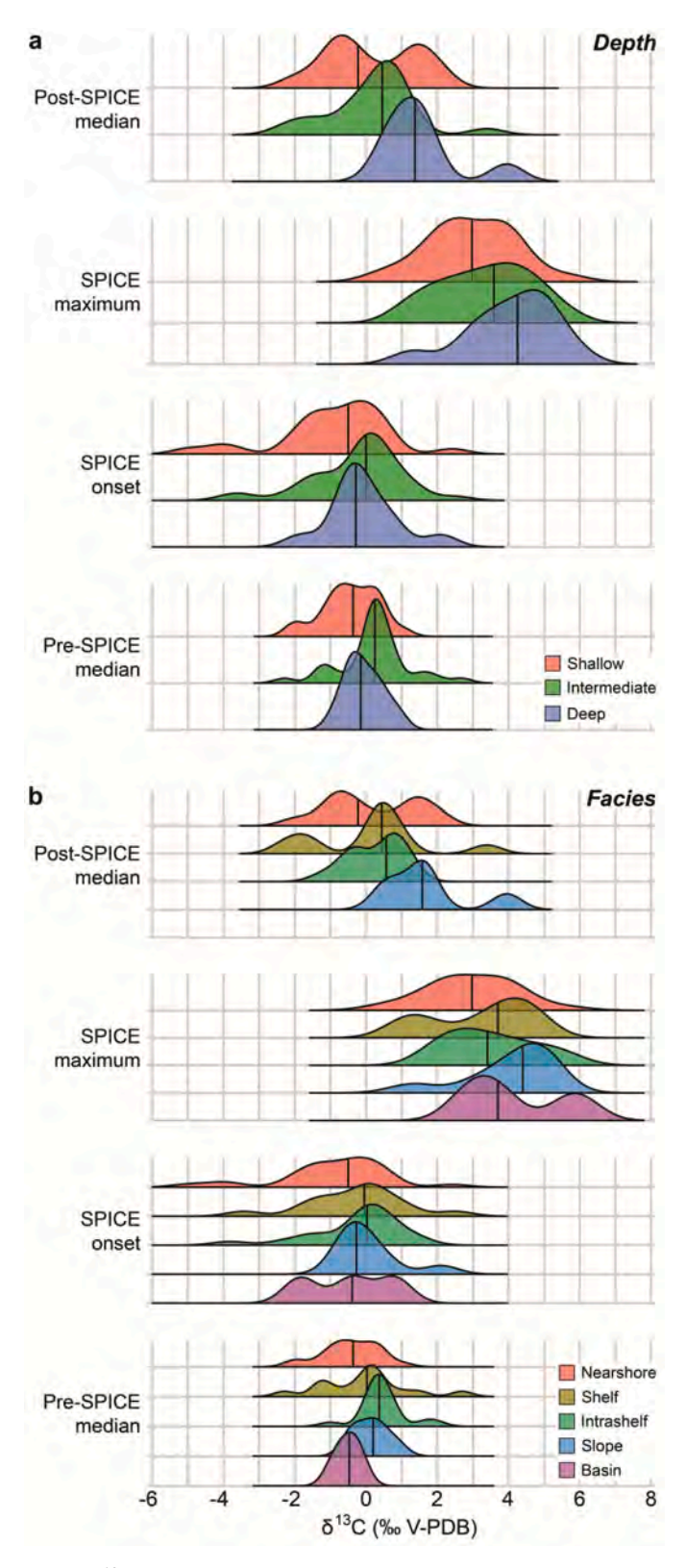


Fig. 10.  $\delta^{13}$ C values before, during, and after the SPICE event. From bottom to top the individual joy plot panels show the distribution in  $\delta^{13}$ C values for the median pre-SPICE background, the minimum of the rising limb (the onset of the SPICE event), the maximum of the rising limb (the peak of the SPICE event), and the median post-SPICE background. The vertical black line within each curve denotes the median value of that distribution. In (a), sections are grouped according to water depth; in (b), sections are grouped according to facies.

(2019) suggest, sea level began to rise (at the beginning of the Sauk III transgression) at or prior to the onset of the rising limb, accommodation space likely would be greater on Laurentia at the time of the SPICEmaximum than on the other paleocontinents. Given that the Sauk megasequence, like all Sloss sequences, is a Laurentia-centric, cratonwide sea level flux package (Sloss, 1963), this could help explain the higher proportion of plateaus (although not statistically significant) in the  $\delta^{13}\text{C}$  excursions of Laurentian sections. More importantly, it is worth noting that these lithostratigraphic relationships documenting the onset of the SPICE during the Sauk III transgression (Schiffbauer et al., 2017; LeRoy and Gill, 2019; Labotka and Freiburg, 2020) run counter to those of other sections showing the excursion beginning during the Sauk II regression (Saltzman et al., 1998, 2004; Glumac and Mutti, 2007; Glumac, 2011)—which can be visualized in Figs. 4-7. This could be a product of deposition in regionally restricted intrashelf basinal paleoenvironments where local tectonic activity overrides the broader Laurentian Sauk sequence signal, or alternatively may imply that the excursion is indeed more asynchronous than perhaps previously accounted for (Schiffbauer et al., 2017).

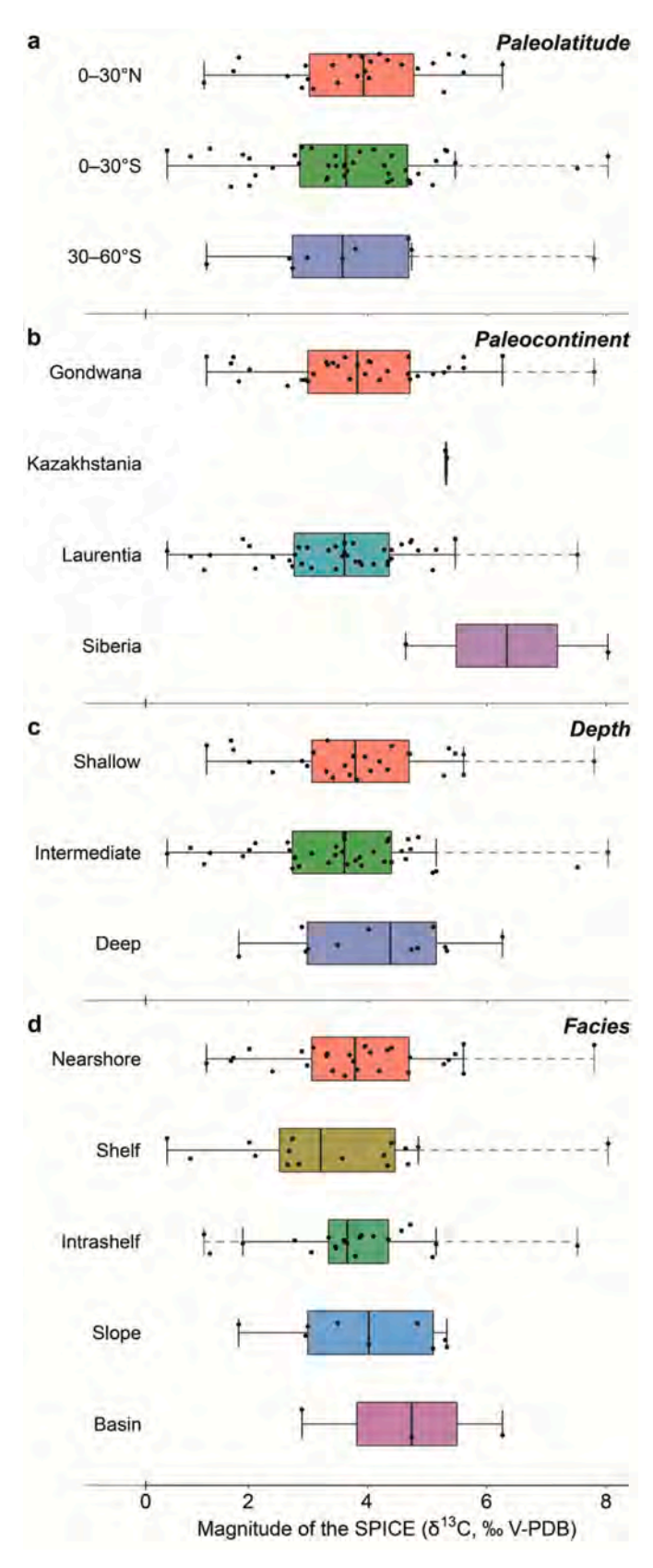
An additional hypothesis also warrants consideration, however. Myrow et al. (2012) investigated the cyclic depositional patterns of Upper Cambrian sections from the Laurentian inner detrital belt. They found that sections in Montana and Wyoming record meter-scale deepening upward packages composed, from bottom to top, of shales, grainstones, flat pebble conglomerates, and thrombolites. These cycles were deposited entirely in subaqueous conditions below fair-weather wave base, within a stable craton; thus, neither tectonic processes nor regional fluctuations in sea level are likely drivers of the observed cyclicity. Rather, Myrow et al. (2012) argue that these cycles are driven by changes in the amount of terrigenous sediment being added to the system as a result of eustatic changes, and the subsequent impact of clastic sediment flux on the carbonate factory. They interpret that the lowermost shale layers were deposited during a regressive period, whereby significant input of siliciclastic material derived from nearby fluvial and shoreline processes caused a reduction in carbonate productivity—and thus are shallow-water shales. As conditions shifted into a transgressive system, siliciclastic input diminished and allowed for the return of carbonate precipitation with increasing quantity and thickness up section, with the uppermost microbial communities developing once waters were devoid of suspended sediment. The topmost beds are sharply capped by the basal shales of the overlying cycle, indicating renewed regression and subsequent suffocation of the carbonate factory (Myrow et al., 2012). Nonetheless, regardless of whether the sections from Schiffbauer et al. (2017), LeRoy and Gill (2019), or others document regression or transgression, these records of the SPICE event appear to be intimately linked to eustatic sea level fluctuations associated with the Sauk II-Sauk III megasequence boundary, although perhaps in a different manner than previously supposed.

## 4.2.2. Pre-SPICE negative excursion

The Marjumiid-Pterocephaliid extinction event is typically described as corresponding to the onset of the rising limb of the SPICE (e.g., Glumac and Walker, 1998; Saltzman et al., 1998; Saltzman et al., 2000; Peng et al., 2004; Gill et al., 2011). The current study documents that most SPICE occurrences are immediately preceded by a relatively small negative carbon isotope excursion (Table 1), contra the assertion by Gerhardt and Gill (2016). Indeed, as observed in Figs. 9 and 10, the negative shift in the left tail of the minimum  $\delta^{13}$ C values for the rising limb relative to the median  $\delta^{13}$ C values for the pre-SPICE baseline suggests that, although not ubiquitous, there is an observable negative  $\delta^{13}$ C "kick" immediately preceding the onset of the SPICE event in perhaps as many as three-quarters of localities (Table 1).

First documented by Saltzman et al. (1995) in the House Range section (entry #24) and later identified by Perfetta et al. (1999) in the Black Hills, South Dakota, United States (entries #S5–S7), this shortlived negative excursion has been suggested to be coincident with the

M.A. Pulsipher et al. Earth-Science Reviews 212 (2021) 103442



(caption on next column)

Fig. 11. Magnitude of the  $\delta^{13}C$  excursion. Box and whisker plots illustrate the magnitude of the  $\delta^{13}C$  excursion captured by the rising limb of the SPICE (maximum  $\delta^{13}C$  value of the rising limb minus the minimum  $\delta^{13}C$  value of the rising limb). Black dots show the magnitude for individual entries. The colored boxes show the interquartile range (IQR = Q3-Q1) of the distribution, with the center black line indicating the median value. Solid line whiskers extend beyond the box by a factor of 1.5 \* IQR, where the upper whisker = min(max (x), Q3 + 1.5 \* IQR) and the lower whisker = max(min(x), Q1-1.5 \* IQR). Dashed line whiskers extend to the absolute minimum or maximum of the distribution, if necessary. Entries are labeled according to the following grouping variables: (a) paleolatitudinal zone; (b) paleocontinent; (c) water-depth; (d) facies.

Marjumiid-Pterocephaliid extinction boundary. In the Black Hills, the magnitude of this negative  $\delta^{13}$ C excursion ranged from 0.48% to 0.78% (increasing magnitude with depth), with a minimum value between -1.10% and -0.40%. Both Saltzman et al. (1995) and Perfetta et al. (1999) ascribed this negative excursion to the influx of cold, deep <sup>12</sup>Cenriched waters into the shallower <sup>13</sup>C-enriched shelf environments where these sections were deposited—where the trilobite extinction boundary is marked by the replacement of the shallow-shelf fauna of the Crepicephalus zone by the deeper-water fauna of the Aphelaspis zone (Stitt, 1975; Palmer, 1984; Saltzman et al., 1995; Perfetta et al., 1999; Palmer et al., 2012; Schiffbauer et al., 2017). It is plausible that the trilobite extinction event was thus correlative with the negative excursion, rather than the transition to the positive excursion as previously proposed. Nonetheless, because it is short-lived and generally small in magnitude, this negative excursion could easily be missed by coarse sampling intervals, thus giving the appearance that the extinction corresponds to the onset of the rising limb of the SPICE. Furthermore, it is not entirely unexpected that an extinction event should correspond to a negative carbon isotope excursion. In a review of mass extinctions and their causes, Bond and Grasby (2017) document 10 Paleozoic extinction events that co-occur with negative  $\delta^{13}\text{C}$  excursions with magnitudes ranging from -2 to -7%, including the end-Permian, end-Triassic, and end-Jurassic extinctions. A biotic crash can lead to a negative  $\delta^{13}$ C excursion; reduced biological activity could cause an enrichment of <sup>12</sup>C in ocean water, pulling the  $\delta^{13}$ C record toward lower values (Saltzman et al., 1995).

One of the important findings by Schiffbauer et al. (2017) was that the record of the SPICE event in Missouri, United States (entries #33-37), is decoupled from trilobite extinction events. Specifically, the onset of the SPICE showed an inconsistent relationship with the Crepicephalus-Aphelaspis turnover and the FAD of Aphelaspis. This is contrary to claims made by others that pin the onset of the SPICE rising limb at the beginning of the Pterocephaliid biomere (e.g., Glumac and Walker, 1998; Saltzman et al., 1998; Saltzman et al., 2000; Peng et al., 2004; Gill et al., 2011; Fig. 1). In a recent contribution, Geyer (2019) presents a comprehensive correlation chart of Cambrian series, biozones, and carbon isotope excursions. The biozone correlation for the regions of interest to this study are redrafted in Fig. 1b for reference. Importantly, Geyer (2019) shows that the timing of the SPICE event is variable. In some regions (Australia, Baltica, Laurentia, North China) the SPICE falls near the base of the Paibian. In other regions, however, the SPICE falls more toward the middle to late Paibian (Kazakhstania, Siberia, South China). Albeit a cursory look at chronostratigraphic placement of the SPICE signal, Geyer's (2019) compilation (Fig. 1b) further corroborates the work by Schiffbauer et al. (2017) and supports the argument that the SPICE event is time-transgressive.

Nevertheless, it is plausible, if not probable, that the Marjumiid-Pterocephaliid extinction event itself is also geologically asynchronous, leaving neither biological turnover nor the SPICE event applicable for precise global correlation. For example, recent work by Sundberg et al. (2020) and Karlstrom et al. (2020) highlight the asynchronous nature of trilobite extinction events. Refined U—Pb detrital zircon ages presented by Karlstrom et al. (2020) indicate that the extinction of

Table 1 Summary table of important  $\delta^{13}$ C values, stratigraphic thicknesses, and metadata for each entry. For both  $\delta^{13}$ C values and stratigraphic thicknesses, all samples marked "Omit" in the SPICEraq were also excluded from these calculations and dashes indicate that a particular SPICE zone was not sampled in that entry. Metadata outlined in this table include paleolatitude, paleocontinent, water depth, simplified facies, and publication reference. See full SPICEraq in SOM for more details, including the name of sections/boreholes. Abbreviations: E# = entry number; Lc = modern geographic location [NA = North America, SA = South America, EU = Europe, AU = Australia]; Pre = pre-SPICE; Rise = rising limb; Plat = plateau; Fall = falling limb; Post = post-SPICE; Exc = Excursion (Rise + Plateau [if present] + Fall); med = median; min = minimum; max = maximum; Fac = facies and Dep = depth [ISB = intrashelf basin, Sh = shallow, NS = nearshore, Int = intermediate, dp = deep]; Lith = lithology [C = "carbonate", L = limestone, D = dolostone]; PCont = paleocontinent [Gond = Gondwana, Kazk = Kazakhstania, Laur = Laurentia, Sib = Siberia]; and PLat° = paleolatitude.

#	Lc	δ <sup>13</sup> C (‰ V	/-PDB)						Stratigraphic thickness (m)							Metadata						
_		Pre med	Rise min	Rise max	Plat med	Fall min	Post med	Pre	Rise	Plat	Fall	Post	Exc	Fac	Dep	Lith	PCont	PLat°	Ref			
	NA	1.64	1.40	5.30	4.63	0.12	0.71	32.80	115.20	44.00	55.00	53.00	214.20	ISB	Int	С	Laur	0-30°N	Baker, 2010			
		0.62	0.32	5.47	4.39	-0.09	0.55	24.00	92.50	77.10	17.20	48.20	186.80	ISB	Int	C	Laur	$0-30^{\circ}S$	Baker, 2010			
		-1.20	-1.10	1.59	1.65	_	_	21.25	5.25	9.00	-	-	14.25	Shelf	Int	D	Laur	30-60°S	Barili et al., 2018			
		-1.23	-1.61	1.13	_	-1.74	-1.53	48.00	22.50	-	7.25	14.50	29.75	Shelf	Int	D	Laur	30-60°S	Barili et al., 2018			
		0.31	-1.20	2.90	_	_	_	26.00	20.00	-	-	-	20.00	ISB	Int	C	Laur	0-30°S	Gerhardt and Gill, 2016			
		0.53	0.40	4.06	_	1.99	_	26.00	19.00	-	4.50	-	23.50	ISB	Int	C	Laur	0-30°S	Gerhardt and Gill, 2016			
		0.37	-3.82	3.70	3.48	_	_	26.25	7.52	7.28	-	-	14.80	ISB	Int	C	Laur	0-30°S	Gerhardt and Gill, 2016			
		0.25	-0.06	3.41	_	_	_	7.00	28.00	-	-	-	28.00	ISB	Int	C	Laur	0-30°S	Gerhardt and Gill, 2016			
		0.17	-0.10	3.77	2.32	-0.32	-0.31	16.80	2.52	4.22	29.28	5.84	36.02	ISB	Int	L	Laur	$0-30^{\circ}S$	Gill et al., 2011			
0		1.48	1.14	3.26	3.65	0.62	0.84	9.14	5.42	53.86	12.74	10.23	72.02	Shelf	Int	L	Laur	0-30°S	Glumac, 2011			
1		2.69	2.51	4.53	4.01	2.34	3.39	2.58	5.89	27.79	4.36	12.94	38.04	Shelf	Int	L	Laur	0-30°S	Glumac, 2011			
2		-0.87	-1.83	2.91	_	1.07	1.25	2.90	2.05	_	1.00	0.10	3.05	Basin	Dp	L	Laur	30-60°S	Glumac and Mutti, 2007			
3		0.33	0.33	4.09	3.18	-0.85	_	10.70	22.80	29.15	30.35	-	82.30	Sh/NS	Sh	L	Laur	0-30°S	Glumac and Walker, 1998			
4		-0.03	0.53	2.94	_	-0.80	-0.85	63.00	20.00	_	16.00	29.00	36.00	Sh/NS	Sh	L	Laur	0-30°S	He, 1995			
5		-1.28	-1.75	1.83	_	-3.00	_	52.14	16.17	_	29.98	_	46.15	Shelf	Int	С	Laur	30-60°S	Hurtgen et al., 2009			
6		_	0.00	4.40	4.40	-2.40	-2.30	_	6.10	7.70	13.80	1.30	27.60	Shelf	Int	D	Laur	0-30°S	Labotka and Freiburg, 202			
7		0.40	-0.50	2.40	_	_	_	59.70	19.10	_	_	_	19.10	Sh/NS	Sh	С	Laur	0-30°S	Laudon, 1992			
8		-0.25	-0.50	3.90	_	_	_	57.50	34.90	_	_	_	34.90	Sh/NS	Sh	С	Laur	0-30°S	Laudon, 1992			
9		0.30	-1.46	2.89	_	_	_	38.13	11.07	_	_	_	11.07	ISB	Int	L	Laur	0-30°S	LeRoy and Gill, 2019			
0		0.56	0.47	1.83	_	_	_	12.60	6.80	_	_	_	6.80	ISB	Int	D	Laur	0-30°S	LeRoy and Gill, 2019			
1		0.70	0.19	2.10	_	_	_	19.30	13.13	_	_	_	13.13	ISB	Int	L	Laur	0-30°S	LeRoy and Gill, 2019			
2		-0.61	-0.30	4.03	3.77	2.94	_	54.00	30.00	20.00	7.00	_	57.00	Shelf	Int	D	Laur	0-30°S	Mackey and Stewart, 2019			
:3		0.72	0.63	1.89	_	0.88	0.99	6.75	3.00	_	4.50	2.25	7.50	ISB	Int	L	Laur	0-30°N	Saltzman et al., 1995			
4		0.57	-0.30	2.76	_	1.07	1.21	25.66	4.84	_	11.50	10.50	16.34	ISB	Int	L	Laur	0-30°S	Saltzman et al., 1995			
5		0.03	0.05	1.08	_	_	_	8.90	12.54	_	_	_	12.54	Shelf	Int	D	Laur	0-30°S	Saltzman et al., 1995			
6		0.35	0.47	1.11	0.92	0.75	_	5.50	2.00	9.50	4.00	_	15.50	Shelf	Int	L	Laur	0-30°S	Saltzman et al., 1995			
7		0.37	0.08	4.65	4.20	0.68	0.70	85.40	165.20	43.10	53.50	28.00	261.80	ISB	Int	L	Laur	0-30°N	Saltzman et al., 1998			
8		1.97	1.39	4.85	4.40	0.37	0.59	76.50	1.50	75.00	21.00	52.10	97.50	ISB	Int	L	Laur	0-30°S	Saltzman et al., 1998			
9		_	0.77	4.38	_	1.11	1.03	_	39.90	_	21.70	43.40	61.60	ISB	Int	L	Laur	0-30°S	Saltzman et al., 1998			
0		_	-1.61	2.19	1.96	-2.27	-1.16	_	29.48	7.46	15.93	38.97	52.87	Shelf	Int	L	Laur	30–60°S	Saltzman et al., 2004			
1		0.90	0.96	3.81	_	0.22	0.47	8.44	6.72	_	7.78	15.29	14.50	Shelf	Int	L	Laur	0-30°S	Saltzman et al., 2004			
2		0.22	-0.10	4.75	3.96	0.05	0.95	24.72	19.02	26.63	16.49	15.69	62.14	Shelf	Int	L	Laur	0-30°S	Saltzman et al., 2004			
3		0.04	0.58	5.67	_	1.66	_	50.29	15.70	_	11.89	_	27.59	ISB	Int	L	Laur	0-30°S	Schiffbauer et al., 2017			
4		0.11	-0.38	2.97	_	-1.46	-0.27	35.36	8.53	_	4.27	27.13	12.80	ISB	Int	D	Laur	0-30°S	Schiffbauer et al., 2017			
5		-1.01	-2.32	2.40	_	-0.99	-0.39	37.79	15.55	_	13.11	13.71	28.66	ISB	Int	D	Laur	0-30°S	Schiffbauer et al., 2017			
6		0.16	0.03	3.64	2.30	-1.09	-0.40	26.52	3.05	16.15	8.38	20.27	27.58	ISB	Int	D	Laur	0-30°S	Schiffbauer et al., 2017			
7		0.18	-0.19	2.59	2.37	_	-	16.31	1.37	11.74	-	_	13.11	ISB	Int	L	Laur	0-30°S	Schiffbauer et al., 2017			
8		-0.45	-1.37	4.10	_	-1.84	-1.13	44.81	2.89	-	7.62	114.61	10.51	Sh/NS	Sh	D	Laur	0-30°S	Jeffrey, 2017			
9		0.25	0.39	4.67	3.68	0.38	0.44	120.09	6.71	39.16	31.09	38.87	76.96	Shelf	Int	D	Laur	0-30°S	Jeffrey, 2017			
0	SA	-1.30	-2.10	5.70	-	-	-	210.90	210.10	-	-	-	210.10	Sh/NS	Sh	L	Gond	30–60°S	Sial et al., 2008			
1	511	-1.50	-0.50	0.80	0.60	-0.90	-0.80	_	28.00	38.70	44.50	59.40	111.20	Sh/NS	Sh	D	Gond	30–60°S	Sial et al., 2013			
2	EU	-2.09	-1.67	3.02	-	-0.89	-0.29	38.70	9.00	-	1.97	20.10	10.97	Sh/NS	Sh	L	Gond	30–60°S	Álvaro et al., 2008			
3	LU	-2.09 -0.70	-0.27	2.72	_	-0.89 -0.99	-0.29 -0.72	37.70	12.30	_	20.00	69.60	32.30	Sh/NS	Sh	C	Laur	30–60°S	Pruss et al., 2019			
4	Asia	0.39	0.15	3.46	_	1.20	-0.72 1.17	3.70	1.10	_	1.75	6.15	2.85	Sh/NS	Sh	L	Gond	0-30°S	Chen et al., 2011			
5	Asia	0.39	0.60	4.10	3.80	1.70	1.70	47.90	18.45	91.20	10.05	26.38	119.70	Slope	Dp	L	Gond	0–30°N	Chung et al., 2011			
6		0.90	-0.80	3.84	J.60 -	-0.83	0.21	1216.00	378.00	91.20	506.00	340.00	884.00	Shelf	Int	C	Sib	0-30°N	Kouchinsky et al., 2008			
7		-0.22	-0.80 -3.43	4.60	_	0.09	0.21	289.10	283.60	_	102.30	508.80	385.90	Shelf	Int	C	Sib	0–30°S	Kouchinsky et al., 2008 Kouchinsky et al., 2008			

(continued on next page)

Table 1 (continued)

<u>E#</u> <u>Lc</u>	δ <sup>13</sup> C (‰ V-PDB)						Stratigraphic thickness (m)							Metadata						
		Pre med	Rise min	Rise max	Plat med	Fall min	Post med	Pre	Rise	Plat	Fall	Post	Exc	Fac	Dep	Lith	PCont	PLat°	Ref	
18		_	-0.27	3.75	-	0.82	-	-	111.00		28.00	-	139.00	Slope	Dp	L	Gond	0-30°N	Li et al., 2018b	
49		_	_	_	_	0.71	_	-	-	-	47.50	-	47.50	Slope	Dp	NA	Gond	$0-30^{\circ}N$	Li et al., 2018b	
50		_	2.10	5.06	-	3.57	3.95	-	88.50	-	7.00	14.50	95.50	Slope	Dp	L	Gond	0-30°N	Li et al., 2018b	
51		0.23	0.15	2.81	1.73	-2.34	-1.84	17.77	7.81	7.84	26.13	1.78	41.78	Shelf	Int	L	Gond	0-30°N	Lim et al., 2015	
52		-2.29	-1.09	3.59	-	0.32	0.46	66.21	19.26	-	23.47	51.77	42.73	Shelf	Int	L	Gond	0-30°S	Liu et al., 2017	
53		1.03	0.52	4.14	_	2.20	2.10	1.30	3.60	-	2.80	3.30	6.40	Sh/NS	Sh	L	Gond	0-30°S	Ng et al., 2014	
54		0.23	-0.53	1.31	_	_	_	177.70	99.80	-	-	-	99.80	Slope	Dp	L	Gond	0-30°N	Saltzman et al., 2000	
55		0.51	0.19	5.03	4.28	1.26	1.66	82.35	150.20	110.25	120.00	230.00	380.45	Slope	Dp	L	Gond	0-30°N	Saltzman et al., 2000	
56		-0.45	-0.51	4.82	_	0.62	0.47	116.00	63.50	-	52.50	208.00	116.00	Slope	Dp	L	Kazk	$0-30^{\circ}S$	Saltzman et al., 2000	
57		-	-0.33	3.87	3.87	2.34	_	-	10.50	11.00	2.70	-	24.20	Sh/NS	Sh	C	Gond	0-30°N	Wang et al., 2020	
58		0.42	-1.00	3.71	_	1.36	1.36	17.90	1.20	-	2.65	7.67	3.85	Sh/NS	Sh	C	Gond	0-30°S	Wang et al., 2020	
9		0.05	0.04	3.37	_	-0.34	1.40	42.70	10.00	-	0.20	4.00	10.20	Sh/NS	Sh	C	Gond	0-30°S	Wang et al., 2020	
0		-	0.55	2.26	_	-	_	-	0.59	-	-	-	0.59	Sh/NS	Sh	C	Gond	0-30°S	Wang et al., 2020	
51		-0.40	-0.30	5.00	_	0.70	0.80	82.10	61.00	-	53.20	19.50	114.20	Slope	Dp	L	Kazk	0-30°S	Wotte and Strauss, 201	
52		0.18	0.21	2.23	_	0.08	0.44	30.10	2.70	_	8.20	35.40	10.90	Sh/NS	Sh	L	Gond	0-30°S	Zhu et al., 2004	
53		0.20	0.00	3.00	_	_	_	124.00	70.50	_	_	_	70.50	Slope	Dp	L	Gond	$0-30^{\circ}N$	Zhu et al., 2004	
54		-0.20	0.80	3.70	3.30	0.90	0.90	108.00	24.00	14.00	21.00	44.00	59.00	Basin	Dp	L	Gond	$0-30^{\circ}N$	Zuo et al., 2018	
55		-0.10	-0.70	4.40	_	0.50	1.50	490.00	150.00	_	125.00	450.00	275.00	Slope	Dp	L	Gond	0-30°N	Zuo et al., 2018	
66	AU	_	2.41	4.16	_	0.97	_	_	127.05	_	131.30	_	258.35	Sh/NS	Sh	L	Gond	0-30°N	Gill et al., 2011	
57		-0.36	-0.05	3.91	_	-0.43	-0.23	166.04	50.93	_	152.10	57.21	203.03	Sh/NS	Sh	C	Gond	0-30°N	Lindsay et al., 2005	
68		-0.47	-0.39	5.87	_	1.04	_	110.65	135.50	_	55.64	_	191.14	Basin	Dp	L	Gond	0-30°N	Saltzman et al., 2000	
59		-0.97	-1.16	1.93	_	-1.30	_	344.42	179.84	_	164.59	_	344.43	Sh/NS	Sh	C	Gond	0-30°N	Schmid, 2017	
70		-1.87	-1.89	1.53	_	-0.12	_	27.44	109.72	_	39.63	_	149.35	Sh/NS	Sh	C	Gond	0-30°N	Schmid, 2017	
71		-0.86	-1.16	2.54	_	-1.29	-1.97	73.15	173.74	_	124.97	164.59	298.71	Sh/NS	Sh	C	Gond	0-30°N	Schmid et al., 2018	
72		-0.31	-0.42	4.86	_	1.12	1.77	50.35	71.95	_	15.40	20.20	87.35	Sh/NS	Sh	D	Gond	$0-30^{\circ}N$	Schmid et al., 2018	
'3		-1.13	-1.32	3.01	_	-2.88	_	64.01	103.63	_	158.50	_	262.13	Sh/NS	Sh	C	Gond	$0-30^{\circ}N$	Schmid et al., 2018	
<b>'</b> 4		-0.75	-1.34	2.49	_	-1.07	_	40.00	140.00	_	100.00	_	240.00	Sh/NS	Sh	C	Gond	$0-30^{\circ}N$	Schmid et al., 2018	
75		_	-3.76	1.85	_	-2.78	_	_	146.30	_	85.34	_	231.64	Sh/NS	Sh	C	Gond	0-30°N	Schmid et al., 2018	
76		_	-5.01	0.35	_	-3.04	_	_	204.21	_	54.87	_	259.08	Sh/NS	Sh	C	Gond	0-30°N	Schmid et al., 2018	
77		-0.71	-1.81	2.24	2.26	1.52	_	90.11	69.17	93.55	11.17	_	173.89	Sh/NS	Sh	C	Gond	$0-30^{\circ}N$	Schmid et al., 2018	
78		_	-4.17	1.44	_	_	_	_	152.30	_	_	_	152.30	Sh/NS	Sh	D	Gond	0-30°N	Schmid et al., 2018	

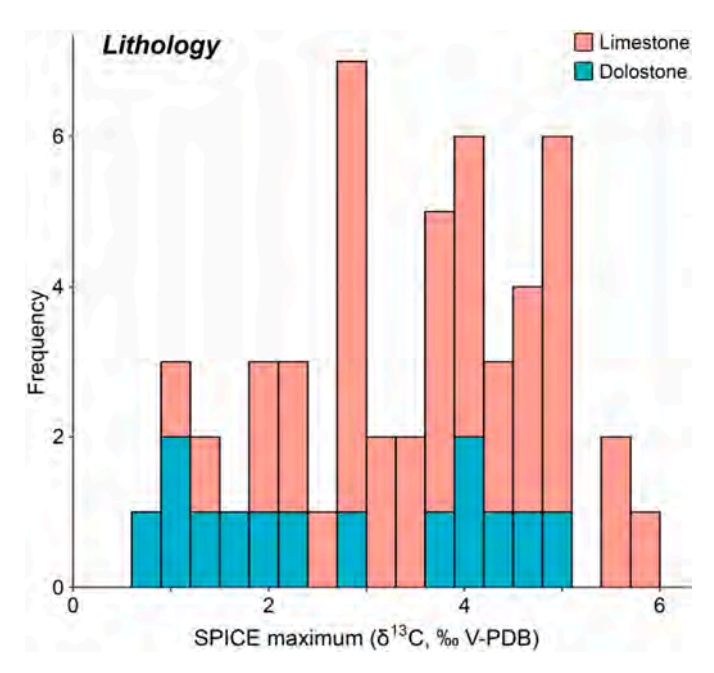


Fig. 12. Influence of lithology on  $\delta^{13}C$  values. This histogram illustrates the distribution of individual maximum  $\delta^{13}C$  values for the rising limb of the SPICE, color-coded by lithology. Samples belonging to the "carbonates" group have been excluded from this figure for visualization purposes. Bin-width = 0.3%, with hard upper boundary.

olenellid- and redlichiid-group trilobites, along with the appearance of paradoxidid-group trilobites, did not occur synchronously at the Series 2-Miaolingian boundary as previously assumed (Sundberg et al., 2020). Rather, these events were asynchronous and protracted, with the FAD of paradoxidids (ca. 509 Ma) notably predating the last appearance datum (LAD) of olenellids (ca. 506.5 Ma), the LAD of redlichiids (ca. 506 Ma), and the Series 2-Miaolingian boundary (506 Ma) by approximately 3 m. y. (Karlstrom et al., 2020; Sundberg et al., 2020). While this example is at the Series boundary prior to the SPICE event at the Miaolingian-Furongian transition, it highlights the need for high-resolution investigation of other trilobite extinction events, as they may be equally as likely to have occurred over similarly protracted time scales rather than as globally synchronous events. However, even if these events are not synchronous on the global-scale, resolving whether or not the Crepicephalus-Aphelaspis turnover co-varies temporally with the SPICE event will be an important step toward resolving any plausible causal relationship.

# 4.2.3. Paleolatitude and paleocontinent

The most consistent trend in  $\delta^{13}$ C data through the SPICE event is observed when sections are grouped by paleolatitude; there are significantly lower  $\delta^{13}$ C values for the 30–60°S sections relative to the more tropical sections located between 30° N and 30° S (Fig. 9a; S7). The correlation between high latitudes and low  $\delta^{13}\text{C}$  values could be due to lower primary productivity in the temperate and polar regions relative to the tropics (e.g., Westberry et al., 2008). Increased biological activity in the lower latitudes regardless of water depth, and more generally in productive shallow coastal ecosystems, could lead to an enrichment of  $^{13}$ C in the water and thus higher  $\delta^{13}$ C values of the carbonates (Knoll et al., 1986; Saltzman et al., 2000). The magnitude of the  $\delta^{13}$ C excursion is fairly consistent across paleolatitudinal zones (Fig. 11a), although smaller magnitude changes are limited to the lower latitude sections, and the highest magnitude changes are limited to the southern hemisphere (Figs. 9a, 11a). One may infer that the consistency in excursion magnitudes across all paleolatitude zones indicates a global nature of the SPICE event, but this would be highly complicated from a chronological perspective as evidenced by the varying relationships with the

Sauk II-Sauk III megasequences and trilobite biomeres. Instead, we suggest that the underlying geochemical signal may be asynchronous and has been filtered through regional/local conditions. Specifically, the paleolatitudinal gradient appears to have a significant effect on the baseline conditions and thus the minimum and maximum  $\delta^{13}$ C values of the rising limb of the SPICE—or effectively, how the SPICE is expressed in the rock record (Table S3a).

The trends observed in the stratigraphic thickness of the SPICE across the paleolatitudinal zones (Figs. 10, S4, S8) are heavily influenced by the geographic position of the paleocontinents (Fig. 2) at 500 Ma, as well as their respective amounts of accommodation space and sediment supply. Sections with the stratigraphically thinnest rising limbs are generally restricted to the Laurentian sections (which is located almost entirely in the southern hemisphere), whereas the stratigraphically thicker sections are restricted generally to Gondwana (which spanned all three paleolatitude zones of interest in this study) and Siberia (which was located dominantly in the 0–30°S zone) (Figs. 2, 8, S4). This further supports the suggestion that Laurentia as a whole had the least amount of accommodation space and/or the lowest sediment supply during the onset of the SPICE, while Siberia had the greatest.

## 4.2.4. Water depth and facies

Generally, deeper water SPICE sections have higher  $\delta^{13}$ C values than shallower water sections, to differing degrees of significance (Figs. 10, 11, and S9; Table S3c–d). With the exception of the extreme outliers #46 and #47, shelf sections host the stratigraphically thinnest excursions overall, and capture the smallest magnitude excursions of all the facies groups (Figs. 8, 11, S4). The minimum magnitudes of the SPICE event show a steady increase with water depth starting with shelf sections, whereas the higher magnitude excursions are limited to shallow and intermediate sections (Fig. 11). The negative excursion immediately preceding the onset of the SPICE is most pronounced in shallow/near-shore sections (Fig. 10). These results support assertions by Schiffbauer et al. (2017), Li et al. (2018b), and Huang et al. (2019) that the stratigraphic expression of the SPICE is dependent on regional/local depositional conditions.

Kump (1991) established a steady-state equation describing the isotopic composition of carbon in surface vs. deep waters. One of the important fluxes in this equation is the input of riverine carbon derived from continental weathering into the surface ocean carbon reservoir. Presuming this carbon flux is depleted in <sup>13</sup>C in the Cambrian, it would have the potential to cause the shallow marine carbon isotope signature to shift toward lower values relative to the deep ocean reservoir. Some authors (e.g., Saltzman et al., 2004; Chen et al., 2011; Wotte and Strauss, 2015; Wang et al., 2020) document increased continental erosion coeval with the onset of the SPICE excursion, which is interpreted to be the result of sea level change. In some sections, this is based on stratigraphic evidence for subaerial exposure (e.g., Saltzman et al., 2004; Chen et al., 2011; Wang et al., 2020) and thus indicates both deposition in shallower water settings and a period of non-deposition. Wotte and Strauss (2015), however, documented high 87Sr/86Sr values in a slope section (entry #61) from Kazakhstan, which suggests an influx of material derived from continental weathering rather than subaerial exposure. In both cases, these lines of evidence document a period of increased continental erosion, which could serve to reduce the  $\delta^{13}$ C values of the shallow water sections by adding a weathered carbon component to the reservoir (Kump, 1991; Wotte and Strauss, 2015). However, in order for continental weathering to have an appreciable effect on local dissolved inorganic carbon (DIC), the depositional setting would need to be proximal to riverine input and/or brackish conditions, not in fully marine conditions.

It is not surprising that regional/local conditions could impact the stratigraphic expression of the SPICE event, and this has likely been the case through much of the history of the planet. Modern ocean waters exhibit heterogeneity in their  $\delta^{13}$ C values that are influenced by many factors (Knoll et al., 1986; Saltzman and Thomas, 2012). For example,

Swart and Eberli (2005) assessed carbon isotope values in a transect of modern sediment cores across the Great Bahamas Bank in water depths ranging from 10 to 650 m. The uppermost portions of the shallowest cores were markedly depleted in <sup>13</sup>C, which they attributed to a reduced influence of pelagic carbonate as well as diagenetic alteration of the sediments by meteoric waters during times of regression and platform exposure. Comparatively, the platform sediments are instead much more enriched in <sup>13</sup>C, likely owing to increased photic zone primary productivity. Likewise, Patterson and Walter (1994) documented a 4‰ decrease in  $\delta^{13}C$  values in modern carbonate platforms of Florida and the Bahamas relative to open ocean waters, again from the input of  $^{13}\mathrm{C}$ depleted terrestrial waters. They concluded that depositional environment is an important consideration in carbon isotope studies because  $\delta^{13}$ C values vary with depth as a result of meteoric influx and evaporation. These modern studies highlight the need for basin-scale lateral investigations in the geologic record in order to more fully appreciate local variability in isotopic signatures.

Other workers have cited early marine diagenesis as the driving force for variation in the geochemical record of carbonates along depth gradients. For example, also from transects across modern carbonate platform and slope environments in the Bahamas, Higgins et al. (2018) document concurrent  $\delta^{13}$ C,  $\delta^{18}$ O,  $\delta^{44}$ Ca, and  $\delta^{26}$ Mg data, with the shallowest water sediments enriched in  $\delta^{44}$ Ca and depleted in  $\delta^{13}$ C values. Similarly, Jones et al. (2020) present  $\delta^{13}$ C,  $\delta^{44}$ Ca, and Sr/Ca data from the Hirnantian isotopic carbon excursion (HICE) in the Upper Ordovician that indicate depth-dependence of the recorded  $\delta^{13}$ C (showing an increase with increasing depth) and  $\delta^{44}$ Ca values (showing a decrease with increasing depth). Both Higgins et al. (2018) and Jones et al. (2020) attribute these results to the variation in the style of early diagenesis that carbonates experience as a result of water depth, depositional environment, and elemental system.

Carbonate diagenesis displays two end-member conditions: fluidbuffered (open diagenesis) or sediment-buffered (closed diagenesis) (Ahm et al., 2018; Higgins et al., 2018; Jones et al., 2020). In fluidbuffered conditions, the chemistry of the diagenetic minerals is controlled by the chemistry of the pore-fluids, which, in carbonate marine environments, is overwhelmingly dominated by seawater. Other types of fluids may certainly affect shallow marine environments; however, the degree to which these fluids may influence the  $\delta^{13}$ C record is likely ultimately dwarfed by the impact that seawater has on fluidbuffered systems on a geologic time scale. In sediment-buffered conditions, the chemistry of the diagenetic minerals is controlled by the chemistry of the primary carbonate minerals. Fluid-buffered conditions dominate in shallow marine environments largely as a result of high rates of fluid flow induced by external processes such a sea-level change (Higgins et al., 2018; Jones et al., 2020). In deeper water environments, where fluid flow-rates are lower, sediment-buffered conditions will prevail (Ahm et al., 2018; Higgins et al., 2018; Jones et al., 2020). Thus, shallow-water carbonates are more likely to record  $\delta^{13}\text{C}$  similar to ambient seawater values as a result of fluid-buffered diagenetic conditions that force sediment geochemistry toward that of seawater (Higgins et al., 2018; Jones et al., 2020). Because the style of early marine diagenesis that affects carbonate deposits is largely controlled by depositional environment water-depth, eustatic sea-level changes can alter the diagenetic conditions of a particular carbonate deposit. Thus, widespread records of correlative  $\delta^{13}$ C excursions may not always indicate global perturbations to the carbon cycle, but instead may record synchronous change in the diagenetic conditions of shallow-water environments driven by eustatic sea-level change (Ahm et al., 2018; Higgins et al., 2018; Jones et al., 2020).

Together, these processes—early marine diagenesis, continental weathering, sea-level change—could help explain the lower  $\delta^{13}$ C values identified here in shallow water sections relative to intermediate and deep-water sections. The greatest isotopic variability in the ocean is confined to the surface ocean reservoir where depositional environments, primary productivity, carbonate precipitation, and other local

environmental factors will have the most appreciable impact (Kump, 1991).

## 4.2.5. Lithology

Of the 52 peak SPICE samples whose lithology could be identified as either limestone or dolostone, limestone samples had a marginally significantly higher median  $\delta^{13} C$  value (Fig. 12; Table S4). The implications of this evaluation are unfortunately limited by the quantity of samples whose lithology could not be refined further than "carbonate," and thus further work is necessary. Regardless, these results do indicate that the specific carbonate chemistry possibly has an appreciable impact on the  $\delta^{13} C$  record, implicating a role for diagenesis in modulating the expression of the SPICE signal, and thus it is important to note the mineralogy of sampled material (i.e., limestone vs. dolostone).

# 4.3. Caveats/assumptions

There are several assumptions associated with the above analyses that need to be mentioned. One important caveat to note is that we are assuming that the stratigraphic sections used in this study are complete, i.e., portions of the rising or falling limbs of the SPICE are not missing due to erosion or any other cause for incompleteness. In a related point, some sections (e.g., entry #3) are missing the falling and/or post-SPICE zones, whereas other sections are missing the pre-SPICE zone (e.g., entry #16). In both instances, the stratigraphic extent and  $\delta^{13}$ C magnitude of the rising limb is compromised and it is possible that they are missing the peak SPICE value and/or the minimum  $\delta^{13}$ C value signaling the onset of the SPICE event. Likewise, our demarcation of a plateau at a minimum stratigraphic thickness of 5 m is notably arbitrary and potentially biases against condensed sections. However, in such cases, we may be competing against poor sampling density for appropriate identification of a plateau. That is, if the distance between individual samples is relatively large versus the overall thickness of the excursion, a plateau may be artificially created simply by the spacing of sampling (e. g., by missing the SPICE peak in collected samples). Admittedly, these are limitations of our study. The total quantity of sections analyzed is sufficiently numerous that it is not feasible to ground-truth the stratigraphic completeness of each section nor to provide additional samples should sampling density be a concern. As such, we must assume that each original publication reports, to the best of the authors' ability, a complete and accurate stratigraphic section with accounts of any observed unconformity or other stratigraphic limitation. We cannot exclude the possibility that the low peak-δ<sup>13</sup>C values and smaller magnitude shifts identified in some sections could be a result of either incomplete sampling or poor sampling density.

Similarly, the significance of our analyses is also affected by the accuracy and completeness of the biostratigraphic framework provided by the original authors. Some sections (e.g., entries #3, #4, #38 [Outcrop 1, Missouri, US; Jeffrey, 2017], #39 [Outcrop 2, Missouri, US; Jeffrey, 2017]) have little to no biostratigraphic control, either because the units contained few fossils or because original fossil fabrics have been obscured by diagenesis. For the majority of the entries, biostratigraphic control relies upon a framework established by previous authors (e.g., entries #22 [Aristech Chemical Corp. #4, Ohio, US; Mackey and Stewart, 2019], and #33-37). Indeed, few studies included in the SPICEraq described collecting their own fossil samples to build a biostratigraphic framework tied to their isotopic analyses (e.g., entry #32 [Saltzman et al., 2004]). Sections with limited fossil control have dubious age constraints and thus prevent us from using the SPICEraq to further evaluate the apparent time-transgressive nature of the SPICE (Schiffbauer et al., 2017; Geyer, 2019). It is possible that sections with sparse fossil evidence may not actually be the correct age to capture the SPICE event and may instead be capturing a preceding or succeeding excursion; however, the entries included in the SPICEraq were all identified as the SPICE by the original authors, and we have taken these interpretations at face value. No attempts were made to re-evaluate

these interpretations based on the fossil evidence described in the original papers.

Lastly, in order to compare individual sections, it was necessary to simplify some of the categorical description included per entry. The first example of this is the relegation of the paleolatitude classifications to a categorical variable, rather than as a quantitative/numerical variable. This was necessitated because not every publication provides precise location metadata for each section, and thus paleolatitudinal coordinates were sometimes approximated by the nearest identifiable city. Had truly quantitative data been uniformly available, for instance, twodimensional density plots could have been used to evaluate more accurate paleolatitudinal trends. Because categorical variables were necessitated, we chose 30°-incremental bins in order to capture ample localities per bin as well as approximate modern climate zones in our resulting analyses. A second simplification is that the facies description of each entry was reduced to a single descriptor. Simplified facies categories were based on in-text descriptions for the majority of samples from the rising limb and plateau zones of the  $\delta^{13}$ C data and applied to all other samples in that entry. Noteworthy examples of this generalization are sections that capture the Nolichucky and Maynardville formations of the Conasauga Group in the Appalachians, United States (entries #5-8 [Gerhardt and Gill, 2016], #10-13 [Glumac, 2011; Glumac and Mutti, 2007; Glumac and Walker, 1998], and #19-21 [LeRoy and Gill, 2019]). The majority of these sections displays an overall shallowing upward trend from the deep ramp, intrashelf basinal facies of the Nolichucky Formation to the shallow marine, peritidal facies of the upper Maynardville Formation (Markello and Read, 1981; Glumac and Walker, 1998). We recognize that this oversimplifies the data by possibly obscuring more detailed variation in the depositional environment and/ or sea level through the progression of the SPICE, and thus likely underestimates the true variability of the SPICE records.

# 4.4. SWEETS entries

When viewed by paleogeographic location (Fig. S2), all SWEETS sections except for one (entry #S13 [Andrarum 3, Sweden; Ahlberg et al., 2009]) are regionally correlative with perhaps less-altered, more savory sections where the SPICE has been positively identified. This may suggest that the absence of an identifiable SPICE signal in the SWEETS sections is not due to a lack of an original excursion in those locations, but rather, several scenarios are plausible: (1) The record of the SPICE was locally masked by diagenetic alteration. (2) The sections are the correct age, but the SPICE event is now absent as a result of a condensed section or erosional activity. Or (3), these sections are not wellconstrained biostratigraphically or geochronologically, and thus the portion of the section sampled for  $\delta^{13}$ C analysis was not time-equivalent to the SPICE. Previous studies such as Saltzman et al. (1998), Glumac and Spivak-Birndorf (2002), Glumac and Mutti (2007), and Pruss et al. (2016) have come to similar conclusions regarding the absence of the SPICE signal in some sections.

# 4.5. The importance of regional/local conditions on the stratigraphic expression of the carbon isotope record

Ocean circulation patterns are difficult to model for the early Phanerozoic because of the vastly different, and still fairly poorly constrained, tectonic plate configuration relative to the modern (Servais et al., 2014). Regardless of the specific details of ancient upwelling zones and surface water currents, the amalgamation of landmasses in the southern hemisphere left a vast open ocean in the northern hemisphere. This, along with differences in Earth's prevailing wind patterns, albedo, and ice cover is likely to have had an appreciable effect on circulation (Brenchley et al., 1994; Saltzman et al., 2000; Servais et al., 2014). It is plausible, if not likely, that the geographic record of the SPICE was affected by these patterns; perhaps the latitudinal variation in the minimum and maximum values of the excursions is a result of this. More

work is necessary to better model ocean circulation patterns of the late Cambrian in order to confirm this and determine what effects it may have had on the global record of the SPICE.

This study is not the first to suggest that regional/local conditions have had an effect on how the SPICE event is recorded. For example, Barili et al. (2018) seconded the idea by Saltzman et al. (2004) that local conditions served as a driving force for the low-magnitude excursion (~ + 2‰) documented at Felix Cove, Newfoundland (entries #3 and #30). Both studies argued that regional tectonics created a restricted, marginal marine environment that became more enriched in <sup>12</sup>C as compared to other locations globally (Saltzman et al., 2004; Barili et al., 2018). In three sections from South China spanning ~650 km, ranging from upper to lower slope depositional environments, the peak of the SPICE event ranges from +3.7 to +5.1% (entries #48–50; Li et al., 2018b); these discrepancies were interpreted as likely due to prolonged ocean stratification as a result of poorly mixed Cambrian seas. Wotte and Strauss (2015) compared a suite of seven SPICE sections from around the globe (entries #9, #15, #27, #29, #61, #66, #68), which included new data they collected as well as previously published data (Saltzman et al., 1998; Saltzman et al., 2000; Gill et al., 2007; Gill et al., 2011), and found that peak  $\delta^{13}$ C values ranged from +1.8% (entry #15; Newfoundland; Hurtgen et al., 2009) to > +6.0% (entry #68; Australia; Saltzman et al., 2000). They similarly concluded that regional conditions led to heterogeneity in the chemical gradients of seawater in the Furongian, and thus the variable  $\delta^{13}$ C records (Wotte and Strauss, 2015). In a case study of five cores (entries #33-37) taken over a paleodepth gradient across ~85 km in southeast Missouri, United States, Schiffbauer et al. (2017) documented that the SPICE event is facies-dependent, time-transgressive, and decoupled from trilobite biotic crises. Thus, the record of the SPICE event displays variation on both local and global scales.

δ<sup>13</sup>C is not the only geochemical signal to display regional variation during the time of the SPICE event. Investigations of paleoredox proxies have documented discrepancies in the timing of peak anoxia relative to extinction events and the  $\delta^{13}C$  maxima in different sections. Positive δ<sup>34</sup>S excursions documented from selected, globally distributed localities exhibit marked variability in both the peak values and the magnitudes of the excursions (Hurtgen et al., 2009; Gill et al., 2011). In the Andrarum-3 drill core from southern Sweden (entry #S13;  $\delta^{13}$ C reported in Ahlberg et al., 2009), paleoredox proxies (reported by Gill et al., 2011), including iron speciation ratios and molybdenum concentrations, indicate persistent euxinic conditions during the SPICE, as well as before and after the excursion. The investigation by LeRoy and Gill (2019) of the Conasauga Intrashelf Basin, Appalachians, United States, however, shows more complexity. Iron speciation data document the presence of anoxic conditions in two shallower sections, although conditions change from euxinic (entry #20) to ferruginous (entry #21) with increasing distance offshore. The most distal Conasauga section does not display any evidence for anoxic conditions, either before or during the onset of the SPICE (LeRoy and Gill, 2019). Using mercury as a paleoredox proxy for the Eilean Dubh Formation (entry #43) in Scotland, Pruss et al. (2019) documented that anoxic conditions began to develop during the rising limb of the SPICE but peaked during the falling limb. Uranium isotope excursions can also be utilized to track the development of anoxic and euxinic conditions globally. Samples from the deep-water Mt. Whelan core (entry #68;  $\delta^{\bar{1}3}$ C reported by Saltzman et al., 2000) in Queensland, Australia indicate that peak anoxic and euxinic conditions are correlative with the trilobite extinction event, but precede the return to baseline values in  $\delta^{13}$ C and  $\delta^{34}$ S proxies (uranium analyses conducted by Dahl et al., 2014).

# 4.6. The utility of the SPICE for global chemostratigraphic correlation

Many workers have used carbon isotope stratigraphy as a method for correlating sections globally through many periods of earth history (e.g., Kaufman et al., 1992; Vahrenkamp, 1996; Ferreri et al., 1997; Saltzman et al., 1998; Saltzman and Thomas, 2012; Voigt et al., 2012). This

method of correlation relies on two fundamental assumptions: (1) that stratigraphic variability in  $\delta^{13}C$  records is the result of secular change in the global marine DIC reservoir; and (2) that excursions in question are synchronous and the result of widespread/global perturbations to the carbon cycle that are relatively unaffected by regional/local conditions during deposition and subsequent diagenesis such that the main signature can still be identified (Saltzman and Thomas, 2012).

We are not arguing the fact that the SPICE event is globally recorded; that is evident in the global distribution of outcrop and core sections bearing records of the SPICE. This study does document, however, that regional/local conditions have a significant impact on the stratigraphic expression of the SPICE event, and presumably on other carbon isotope excursions as well. The variability in  $\delta^{13} C$  records documented in this study suggests that there is the possibility that other records of the SPICE event may have gone unrecognized because they do not fit the typical description of the excursion. Smaller magnitude or shorter stratigraphic records of the SPICE could be misidentified as a different excursion or missed entirely by coarse sampling densities. Similarly, inadequate fossil control and the time-transgressive nature of the excursion presents the possibility that some identified SPICE sections are not actually representative of the SPICE event. Attempts should be made to give more attention to the context of chemostratigraphic excursions beyond the magnitude of their rising limb, and several key questions can be posed. For instance, how are the segments of the excursion expressed over stratigraphic thickness? How do lithologic or diagenetic changes in the strata relate to the expression of the excursion? How do excursions from new sampling locations relate to the results of regional/global metaanalyses? Addressing these questions moving forward may allow for a greater understanding of processes leading to the patterns observed and may additionally generate new testable hypotheses as opposed to relying on pattern-matching or biostratigraphy alone.

## 5. Conclusions

In summary, emergent trends are identified from a meta-analysis of 78 globally distributed stratigraphic sections that record the SPICE event.

- Sections deposited between 30 and  $60^{\circ}$ S paleolatitude have consistently lower  $\delta^{13}$ C values throughout the SPICE than those sections deposited in the tropics. This may result from reduced primary productivity and/or colder water temperatures at higher latitudes.
- Shallow water sections tend to have lower  $\delta^{13}C$  values than sections from deeper water environments. This trend is likely driven by the differing diagenetic conditions experienced by shallow- and deepwater carbonates and is related to the Sauk II-Sauk III transition.
- Host-rock lithology, i.e., limestone versus dolostone, appears to have an appreciable effect on the recording of  $\delta^{13} \text{C}$  during the SPICE, implicating a role for diagenesis in modulating the expression of the SPICE signal. As such, it is important to note the mineralogy of sampled material when measuring and reporting carbon isotopic data.
- Regional/local conditions have a significant impact on the stratigraphic expression of the SPICE event and presumably other carbon isotope excursions.
- There is an identifiable negative  $\delta^{13}C$  excursion immediately preceding the onset of the SPICE in the majority of the entries included in the SPICEraq. Thus, this negative excursion may be global in nature; its absence from some sections could be an artifact of sampling density or erosional activity.
- The apparent time-transgressive nature of the SPICE challenges assumptions that it is mediated by a change in the isotopic composition of marine DIC, which would impact all sections synchronously.

## **Author contributions**

Following the CRediT model: MAP is responsible for data mining, compilation, and curation of the SPICEraq, as well as software processing and statistical analyses. JDS is responsible for provision of resources, project supervision, and project administration. JDS, JWH, and KLS jointly conceived the project. Funding acquisition to support the project was obtained by KLS and JDS. MAP and JDS are jointly responsible for preparing the original draft of the manuscript and data visualization, with initial review and edits provided by KLS, DAF, and JWH. MJJ and KLS collected additional field- and core-samples from southeast Missouri, which were processed by DAF. JWH assisted with and oversaw statistical analyses. MAP and JDS prepared the final versions of the manuscript and supplement, with substantial input from all of the authors.

# **Declaration of Competing Interest**

The authors declare that they have no known competing financial interests or personal relationships that could have appeared to influence the work reported in this paper.

# Acknowledgments

The authors would like to thank P. Scheel and the staff at the McCracken Core Library and Research Center, Missouri Department of Natural Resources for core access and assistance, S. Jacquet (Univ. of Missouri) for sample collection assistance, S. Moore (Washington Univ. in St. Louis) for IRMS processing, and S. Rosbach (Univ. of Missouri) for RStudio assistance. We additionally thank M. Brown, M. Chisholm, V. Beckham, E. Bunton, and G. Halliwell for project inspiration. Funding: This work was supported by the Univ. of Missouri Research Council to KLS; the Univ. of Missouri Dept. of Geological Sciences to MAP [James H. Stitt Memorial Fellowship, Keller Opportunities for Excellence, and Marshall Opportunities for Excellence]; the National Science Foundation to JDS [EAR CAREER #1652351] and JWH [EAR CAREER #1650745].

# Appendix A. Supplementary data

Supplementary data to this article can be found online at https://doi.org/10.1016/j.earscirev.2020.103442.

# References

- Ahlberg, P., Axheimer, N., Babcock, L.E., Eriksson, M.E., Schmitz, B., Terfelt, F., 2009. Cambrian high-resolution biostratigraphy and carbon isotope chemostratigraphy in Scania, Sweden: first record of the SPICE and DICE excursions in Scandinavia. Lethaia 42, 2–16. https://doi.org/10.1111/j.1502-3931.2008.00127.x.
- Ahlberg, P., Lundberg, F., Erlström, M., Calner, M., Lindskog, A., Dalhqvist, P., Joachimski, M.M., 2019. Integrated Cambrian biostratigraphy and carbon isotope chemostratigraphy of the Grönhögen-2015 drill core, Öland, Sweden. Geol. Mag. 156, 935–949. https://doi.org/10.1017/S0016756818000298.
- Ahm, A.S.C., Bjerrum, C.J., Blättler, C.L., Swart, P.K., Higgins, J.A., 2018. Quantifying early marine diagenesis in shallow-water carbonate sediments. Geochim. Cosmochim. Acta 236, 140–159. https://doi.org/10.1016/j.gca.2018.02.042.
- Álvaro, J.J., Bauluz, B., Subias, I., Pierre, C., Vizcaino, D., 2008. Carbon chemostratigraphy of the Cambrian-Ordovician transition in a midlatitude mixed platform, Montagne Noire, France. Geol. Soc. Am. Bull. 120, 962–975. https://doi. org/10.1130/B26243.1.
- Auerbach, D.J., 2004. The Steptoean Positive Isotopic Carbon Excursion (SPICE) in Siliciclastic Facies of the Upper Mississippi Valley: Implications for Mass Extinction and Sea Level Change in the Upper Cambrian. Carleton College.
- Azmy, K., 2019. Carbon-isotope stratigraphy of the SPICE event (Upper Cambrian) in eastern Laurentia: implications for global correlation and a potential reference section. Geol. Mag. 156, 1311–1322. https://doi.org/10.1017/ S0016756818000638.
- Baker, J.L., 2010. Carbon Isotopic Fractionation Across a Late Cambrian Carbonate Platform: A Regional Response to the SPICE Event as Recorded in the Great Basin (M. S. thesis). University of Nevada, Las Vegas.
- Barili, R., Neilson, J.E., Brasier, A.T., Goldberg, K., Pastro Bardola, T., De Ros, L.F., Leng, M., 2018. Carbon isotopes, stratigraphy, and environmental change: the

- Middle-Upper Cambrian positive excursion (SPICE) in Port au Port Group, western Newfoundland, Canada. Can. J. Earth Sci. 55, 1209–1222. https://doi.org/10.1139/ciec.2019.025
- Bond, D.P.G., Grasby, S.E., 2017. On the causes of mass extinctions. Palaeogeogr. Palaeoclimatol. Palaeoecol. 478, 3–29. https://doi.org/10.1016/j.palaeo.2016.11.005.
- Brasier, M.D., 1993. Towards a carbon isotope stratigraphy of the Cambrian System: potential of the Great Basin succession. Geol. Soc. London Spec. Publ. 70, 341–350. https://doi.org/10.1144/GSL.SP.1993.070.01.22.
- Brenchley, P.J., Marshall, J.D., Carden, G.A.F., Robertson, D.B.R., Long, D.G.F., Meidla, T., Hints, L., Anderson, T.F., 1994. Bathymetric and isotopic evidence for a short-lived late Ordovician glaciation in a greenhouse period. Geology 22, 295–298. https://doi.org/10.1130/0091-7613(1994)022<0295:BAIEFA>2.3.CO;2.
- Buggisch, W., Keller, M., Lehnert, O., 2003. Carbon isotope record of late Cambrian to early Ordovician carbonates of the argentine Precordillera. Palaeogeogr. Palaeoclimatol. Palaeoecol. 195, 357–373. https://doi.org/10.1016/S0031-0182 (03)00365-1.
- Chen, J., Chough, S.K., Han, Z., Lee, J.-H., 2011. An extensive erosion surface of a strongly deformed limestone bed in the Gushan and Chaomidian formations (late Middle Cambrian to Furongian), Shandong Province, China: Sequence–stratigraphic implications. Sediment. Geol. 233, 129–149. https://doi.org/10.1016/j. sedgep. 2010.11.002
- Chung, G.-S., Lee, J.-G., Lee, K.-S., 2011. Stable Carbon Isotope Stratigraphy of the Cambrian Machari Formation in the Yeongweol Area, Gangweon Province, Korea. J. Korean Earth Sci. Soc. 32, 437–452. https://doi.org/10.5467/ JKFSS 2011.32.5.437
- Cowan, C.A., Fox, D.L., Runkel, A.C., Saltzman, M.R., 2005. Terrestrial-marine carbon cycle coupling in ~500-m.y.-old phosphatic brachiopods. Geology 33, 661. https:// doi.org/10.1130/G21434.1.
- Dahl, T.W., Boyle, R.A., Canfield, D.E., Connelly, J.N., Gill, B.C., Lenton, T.M., Bizzarro, M., 2014. Uranium isotopes distinguish two geochemically distinct stages during the later Cambrian SPICE event. Earth Planet. Sci. Lett. 401, 313–326. https://doi.org/10.1016/j.epsl.2014.05.043.
- Dilliard, K.A., Pope, M.C., Coniglio, M., Hasiotis, S.T., Lieberman, B.S., 2007. Stable isotope geochemistry of the lower Cambrian Sekwi Formation, Northwest Territories, Canada: implications for ocean chemistry and secular curve generation. Palaeogeogr. Palaeoclimatol. Palaeoecol. 256, 174–194. https://doi.org/10.1016/j.palaeo.2007.02.031.
- Elrick, M., Rieboldt, S., Saltzman, M., McKay, R.M., 2011. Oxygen-isotope trends and seawater temperature changes across the late Cambrian Steptoean Positive Carbon-Isotope Excursion (SPICE event). Geology 39, 987–990. https://doi.org/10.1130/ G32109.1.
- Ferreri, V., Weissert, H., D'Argenio, B., Buonocunto, F.P., 1997. Carbon isotope stratigraphy: a tool for basin to carbonate platform correlation. Terra Nova 9, 57–61. https://doi.org/10.1111/j.1365-3121.1997.tb00002.x.
- Gerhardt, A.M., 2014. Carbon Cycle Changes during the End-Marjuman (Cambrian) Extinction in the Southern Appalachians. Virginia Polytechnic Institute and State University.
- Gerhardt, A.M., Gill, B.C., 2016. Elucidating the relationship between the later Cambrian end-Marjuman extinctions and SPICE Event. Palaeogeogr. Palaeoclimatol. Palaeoecol. 461, 362–373. https://doi.org/10.1016/j.palaeo.2016.08.031.
- Geyer, G., 2019. A comprehensive Cambrian correlation chart. Episodes 42, 321–332. https://doi.org/10.18814/epiiugs/2019/019026.
- Gill, B.C., Lyons, T.W., Saltzman, M.R., 2007. Parallel, high-resolution carbon and sulfur isotope records of the evolving Paleozoic marine sulfur reservoir. Palaeogeogr. Palaeoclimatol. Palaeoecol. 256, 156–173. https://doi.org/10.1016/j. palaeo.2007.02.030.
- Gill, B.C., Lyons, T.W., Young, S.A., Kump, L.R., Knoll, A.H., Saltzman, M.R., 2011. Geochemical evidence for widespread euxinia in the later Cambrian Ocean. Nature 469, 80–83. https://doi.org/10.1038/nature09700.
- Glumac, B., 2011. High-resolution stratigraphy and correlation of Cambrian strata using carbon isotopes: an example from the southern Appalachians, USA. Carbonates Evaporites 26, 287–297. https://doi.org/10.1007/s13146-011-0065-2.
- Glumac, B., Mutti, L.E., 2007. Late Cambrian (Steptoean) sedimentation and responses to sea-level change along the northeastern Laurentian margin: Insights from carbon isotope stratigraphy. Geol. Soc. Am. Bull. 119, 623–636. https://doi.org/10.1130/ R25807 1
- Glumac, B., Spivak-Birndorf, M.L., 2002. Stable isotopes of carbon as an invaluable stratigraphic tool: an example from the Cambrian of the northern Appalachians, USA. Geology 30, 563. https://doi.org/10.1130/0091-7613(2002)030<0563: SIOCAA>2.0.CO;2.
- Glumac, B., Walker, K.R., 1998. A late Cambrian positive carbon-isotope excursion in the Southern Appalachians; relation to biostratigraphy, sequence stratigraphy, environments of deposition, and diagenesis. J. Sediment. Res. 68, 1212–1222. https://doi.org/10.2110/jsr.68.1212.
- Hammer, Ø., Harper, D.A.T., Ryan, P.D., 2001. PAST: paleontological statistics software package for education and data analysis. Palaeontol. Electron. 4, 9.
- Harper, D.A.T., Topper, T.P., Cascales-Miñana, B., Servais, T., Zhang, Y.-D., Ahlberg, P., 2019. The Furongian (late Cambrian) Biodiversity Gap: real or apparent? Palaeoworld 28, 4–12. https://doi.org/10.1016/j.palwor.2019.01.007.
- He, Z., 1995. Sedimentary Facies and Variation of Stable Isotope Composition of Upper Cambrian to Lower Ordovician Strata in Southern Missouri: Implications for the Origin of MVT Deposits, and the Geochemical and Hydrological Features of Regional Ore-forming Fluids (Ph.D. dissertation). University of Missouri-Rolla, p. 124.
- He, Z., Gregg, J.M., Shelton, K.L., Palmer, J.R., 1997. Sedimentary facies control of fluid flow and mineralization in Cambro-Ordovician strata, Southern Missouri. In: Basin-

- Wide Diagenetic Patterns: Integrated Petrologic, Geochemical, and Hydrological Considerations. SEPM Special Publication No. 57.
- Higgins, J.A., Blättler, C.L., Lundstrom, E.A., Santiago-Ramos, D.P., Akhtar, A.A., Crüger Ahm, A.S., Bialik, O., Holmden, C., Bradbury, H., Murray, S.T., Swart, P.K., 2018. Mineralogy, early marine diagenesis, and the chemistry of shallow-water carbonate sediments. Geochim. Cosmochim. Acta 220, 512–534. https://doi.org/10.1016/j.gra.2017.09.046
- Huang, J., Chen, Y., Chu, X., Sun, T., 2019. The geochemistry of the late Cambrian carbonate in North China: the Steptoean Positive Carbon Isotope Excursion (SPICE) record suppressed in a coastal condition? Geol. Mag. 156, 1805–1819. https://doi. org/10.1017/S0016756819000025.
- Hurtgen, M.T., Pruss, S.B., Knoll, A.H., 2009. Evaluating the relationship between the carbon and sulfur cycles in the later Cambrian Ocean: an example from the Port au Port Group, western Newfoundland, Canada. Earth Planet. Sci. Lett. 281, 288–297. https://doi.org/10.1016/j.epsl.2009.02.033.
- Jeffrey, M.J., 2017. Stratigraphic Variation of the Late Cambrian SPICE Event in Upper Cambrian Carbonates of Southern Missouri (M.S. thesis). University of Missouri-Columbia
- Jeffrey, M.J., Huntley, J.W., Schiffbauer, J.D., Fike, D.A., Shelton, K.L., 2017. Influences of environmental variation and sedimentation rate on the recording of the Steptoean Positive Carbon Isotope Excursion (SPICE) in Missouri. In: GSA Program with Abstracts, p. 300613. https://doi.org/10.1130/abs/2017AM-300613.
- Jones, D.S., Brothers, R.W., Ahm, A.S.C., Slater, N., Higgins, J.A., Fike, D.A., 2020. Sea level, carbonate mineralogy, and early diagenesis controlled 8<sup>13</sup>C records in Upper Ordovician carbonates. Geology 48, 194–199. https://doi.org/10.1130/G46861.1.
- Karlstrom, K.E., Mohr, M.T., Schmitz, M.D., Sundberg, F.A., Rowland, S.M., Blakey, R., Foster, J.R., Crossey, L.J., Dehler, C.M., Hagadorn, J.W., 2020. Redefining the Tonto Group of Grand Canyon and recalibrating the Cambrian time scale. Geology 48, 425–430. https://doi.org/10.1130/G46755.1.
- Kaufman, A.J., Knoll, A.H., Awramik, S.M., 1992. Biostratigraphic and chemostratigraphic correlation of Neoproterozoic sedimentary successions: upper Tindir Group, northwestern Canada, as a test case. Geology 20, 181. https://doi.org/ 10.1130/0091-7613(1992)020<0181:BACCON>2.3.CO;2.
- Knoll, A.H., Hayes, J.M., Kaufman, A.J., Swett, K., Lambert, I.B., 1986. Secular variation in carbon isotope ratios from Upper proterozoic successions of Svalbard and East Greenland. Nature 321, 832–838. https://doi.org/10.1038/321832a0.
- Kouchinsky, A., Bengton, S., Gallet, Y., Korovnikov, I., Pavlov, V., Runnegar, B., Shields, G., Veizer, J., Young, E., Ziegler, K., 2008. The SPICE carbon isotope excursion in Siberia: a combined study of the upper Middle Cambrian–lowermost Ordovician Kulyumbe River section, northwestern Siberian Platform. Geol. Mag. 145, 609–622. https://doi.org/10.1017/S0016756808004913.
- Kump, L.R., 1991. Interpreting carbon-isotope excursions: Strangelove oceans. Geology 19, 299. https://doi.org/10.1130/0091-7613(1991)019<0299:ICIESO>2.3.CO:2.
- Labotka, D.M., Freiburg, J.T., 2020. Geochemical preservation of the Steptoean Positive Carbon Isotope Excursion (SPICE) event in dolomites of the Furongian Franconia Formation in the Illinois Basin. Illinois State Geol. Surv. Circular 6, 11.
- Laudon, P.R., 1992. Dolomite Neomorphism and Water-rock Relationships in the Mineralized Bonneterre Dolomite (Cambrian), Southeast Missouri (M.S. thesis). University of Missouri-Rolla, p. 165.
- LeRoy, M.A., Gill, B.C., 2019. Evidence for the development of local anoxia during the Cambrian SPICE event in eastern North America. Geobiology 17, 381–400. https://doi.org/10.1111/gbi.12334.
- Li, W., Jia, P., Fan, R., Lu, Y., Li, X., Deng, S., 2018a. Carbon isotope characteristics of the Middle–Upper Cambrian Xixiangchi Group and bottom boundary marks of Furongian Series in the Sichuan Basin and its adjacent areas. Nat. Gas Ind. B 5, 177–184. https://doi.org/10.1016/j.ngib.2018.04.004.
- Li, D., Zhang, Xiaolin, Hu, D., Chen, X., Huang, W., Zhang, Xu, Li, M., Qin, L., Peng, S., Shen, Y., 2018b. Evidence of a large δ<sup>13</sup>C<sub>carb</sub> and δ<sup>13</sup>C<sub>org</sub> depth gradient for deepwater anoxia during the late Cambrian SPICE event. Geology 46, 631–634. https://doi.org/10.1130/G40231.1.
- Lim, J.N., Chung, G.S., Park, T.-Y.S., Lee, K.S., 2015. Lithofacies and stable carbon isotope Stratigraphy of the Cambrian Sesong formation in the Taebaeksan Basin, Korea. J. Korean Earth Sci. Soc. 36, 617–631. https://doi.org/10.5467/ JKESS.2015.36.7.617.
- Lindsay, J.F., Kruse, P.D., Green, O.R., Hawkins, E., Brasier, M.D., Cartlidge, J., Corfield, R.M., 2005. The Neoproterozoic-Cambrian record in Australia: a stable isotope study. Precambrian Res. 143, 113–133. https://doi.org/10.1016/j. precamres.2005.10.002.
- Liu, H., Liao, Z., Zhang, H., Tian, Y., Cheng, B., Yang, S., 2017. Stable isotope (δ<sup>13</sup>C<sub>ker</sub>, δ<sup>13</sup>C<sub>carb</sub>, δ<sup>18</sup>O<sub>carb</sub>) distribution along a Cambrian outcrop section in the eastern Tarim Basin, NW China and its geochemical significance. Geosci. Front. 8, 163–170. https://doi.org/10.1016/j.gsf.2016.02.004.
- Mackey, J.E., Stewart, B.W., 2019. Evidence of SPICE-related anoxia on the Laurentian passive margin: Paired δ<sup>13</sup>C and trace element chemostratigraphy of the upper Conasauga Group, Central Appalachian Basin. Palaeogeogr. Palaeoclimatol. Palaeoecol. 528, 160–174. https://doi.org/10.1016/j.palaeo.2019.04.018.
- Maloof, A.C., Schrag, D.P., Crowley, J.L., Bowring, S.A., 2005. An expanded record of early Cambrian carbon cycling from the Anti-Atlas margin, Morocco. Can. J. Earth Sci. 42, 2195–2216. https://doi.org/10.1139/e05-062.
- Markello, J.R., Read, J.F., 1981. Carbonate ramp-to-deeper shale shelf transitions of an Upper Cambrian intrashelf basin, Nolichucky Formation, Southwest Virginia Appalachians. Sedimentology 28, 573–597. https://doi.org/10.1111/j.1365-3091.1981.tb01702.x.
- Melchin, M.J., Mitchell, C.E., Holmden, C., Štorch, P., 2013. Environmental changes in the late ordovician-early silurian: Review and new insights from black shales and

- nitrogen isotopes. Bull. Geol. Soc. Am. 125, 1635–1670. https://doi.org/10.1130/
- Müller, R.D., Cannon, J., Qin, X., Watson, R.J., Gurnis, M., Williams, S., Pfaffelmoser, T., Seton, M., Russell, S.H.J., Zahirovic, S., 2018. GPlates: building a Virtual Earth through Deep Time. Geochem. Geophys. Geosyst. 19, 2243–2261. https://doi.org/ 10.1029/2018GC007584.
- Myrow, P.M., Taylor, J.F., Runkel, A.C., Ripperdan, R.L., 2012. Mixed siliciclasticcarbonate upward-deepening cycles of the upper Cambrian inner detrital belt of laurentia. J. Sediment. Res. 82, 216–231. https://doi.org/10.2110/jsr.2012.20.
- Ng, T.-W., Yuan, J.-L., Lin, J.-P., 2014. The North China Steptoean Positive Carbon Isotope Event: new insights towards understanding a global phenomenon. Geobios 47, 371–387. https://doi.org/10.1016/j.geobios.2014.09.003.
- Palmer, A.R., 1984. The biomere problem: evolution of an idea. J. Paleontol. 58, 599–611.
- Palmer, J., Thompson, T.L., Seeger, C., Miller, J.F., Gregg, J.M., 2012. The Sauk Megasequence from the Reelfoot Rift to Southwestern Missouri. Gt. Am. Carbonate bank Geol. Econ. Resour. 1013–1030. https://doi.org/10.1306/13331527M983518. Cambrian-Ordovician Sauk megasequence Laurentia AAPG Memoi.
- Patterson, W.P., Walter, L.M., 1994. Depletion of <sup>13</sup>C in seawater ΣCO<sub>2</sub> on modern carbonate platforms: significance for the carbon isotopic record of carbonates. Geology 22, 885. https://doi.org/10.1130/0091-7613(1994)022<0885: DOCISC>2.3.CO:2.
- Peng, S., Babcock, L., Robison, R., Lin, H., Rees, M., Saltzman, M., 2004. Global Standard Stratotype-section and Point (GSSP) of the Furongian Series and Paibian Stage (Cambrian). Lethaia 37, 365–379. https://doi.org/10.1080/00241160410002081.
- Peng, Y., Peng, Y., Lang, X., Ma, H., Huang, K., Li, F., Shen, B., 2016. Marine carbon-sulfur biogeochemical cycles during the Steptoean Positive Carbon Isotope Excursion (SPICE) in the Jiangnan Basin, South China. J. Earth Sci. 27, 242–254. https://doi.org/10.1007/s12583-016-0694-4.
- Perfetta, P.J., Shelton, K.L., Stitt, J.H., 1999. Carbon isotope evidence for deep-water invasion at the Marjumiid-Pterocephaliid biomere boundary, Black Hills, USA: a common origin for biotic crises on late Cambrian shelves. Geology 27, 403–406. https://doi.org/10.1130/0091-7613(1999)027<0403:CIEFDW>2.3.CO;2.
- Pruss, S.B., Castagno, K.A., Fike, D.A., Hurtgen, M.T., 2016. Carbon isotope (8<sup>13</sup>C<sub>carb</sub>) heterogeneity in deep-water Cambro-Ordovician carbonates, western Newfoundland. Palaeogeogr. Palaeoclimatol. Palaeoecol. 458, 52–62. https://doi.org/10.1016/j.palaeo.2015.10.004.
- Pruss, S.B., Jones, D.S., Fike, D.A., Tosca, N.J., Wignall, P.B., 2019. Marine anoxia and sedimentary mercury enrichments during the late Cambrian SPICE event in northern Scotland. Geology 47, 475–478. https://doi.org/10.1130/G45871.1.
- R Core Team, 2019. R: A language and environment for statistical computing. R foundation for Statistical Computing, Vienna, Austria. https://www.R-project.org/. Rohatgi, A., 2019. WebPlot Digitizer (Version 4.2) [Computer software]. https://automeris.io/WebPlotDigitizer (accessed 16 March 2020).
- Rose, C.V., Fischer, W.W., Finnegan, S., Fike, D.A., 2019. Records of carbon and sulfur cycling during the Silurian Ireviken Event in Gotland, Sweden. Geochim. Cosmochim. Acta 246, 299–316. https://doi.org/10.1016/j.gca.2018.11.030.
- Saltzman, M.R., Thomas, E., 2012. Carbon Isotope Stratigraphy. In: Gradstein, F.M., Ogg, J.G., Schmitz, M.D., Ogg, G.M. (Eds.), The Geologic Time Scale. Elsevier, pp. 207–232. https://doi.org/10.1016/B978-0-444-59425-9.00011-1.
- Saltzman, M.R., Cowan, C.A., Runkel, A.C., Runnegar, B., Stewart, M.C., Palmer, A.R., 2004. The late Cambrian SPICE (8<sup>13</sup>C) event and the Sauk II-Sauk III regression: new evidence from Laurentian basins in Utah, Iowa, and Newfoundland. J. Sediment. Res. 74, 366–377. https://doi.org/10.1306/120203740366.
- Saltzman, M.R., Davidson, J.P., Holden, P., Runnegar, B., Lohmann, K.C., 1995. Sealevel-driven changes in ocean chemistry at an Upper Cambrian extinction horizon. Geology 23, 893. https://doi.org/10.1130/0091-7613(1995)023<0893: SLDCIO>2.3.CO:2.
- Saltzman, M.R., Runnegar, B., Lohmann, K.C., 1998. Carbon isotope stratigraphy of Upper Cambrian (Steptoean Stage) sequences of the eastern Great Basin: Record of a global oceanographic event. Geol. Soc. Am. Bull. 110, 285–297. https://doi.org/ 10.1130/0016-7606(1998)110<0285:CISOUC>2.3.CO:2.
- Saltzman, M.R., Ripperdan, R.L., Brasier, M.D., Lohmann, K.C., Robison, R.A., Chang, W. T., Peng, S., Ergaliev, E.K., Runnegar, B., 2000. A global carbon isotope excursion (SPICE) during the late Cambrian: relation to trilobite extinctions, organic-matter burial and sea level. Palaeogeogr. Palaeoclimatol. Palaeoceocl. 162, 211–223. https://doi.org/10.1016/S0031-0182(00)00128-0.
- Saltzman, M.R., Young, S.A., Kump, L.R., Gill, B.C., Lyons, T.W., Runnegar, B., 2011.
  Pulse of atmospheric oxygen during the late Cambrian. Proc. Natl. Acad. Sci. 108, 3876–3881. https://doi.org/10.1073/pnas.1011836108.
- Schiffbauer, J.D., Huntley, J.W., Fike, D.A., Jeffrey, M.J., Gregg, J.M., Shelton, K.L., 2017. Decoupling biogeochemical records, extinction, and environmental change during the Cambrian SPICE event. Sci. Adv. 3, e1602158 https://doi.org/10.1126/ sciadv.1602158.
- Schlager, W., 1993. Accommodation and supply—a dual control on stratigraphic sequences. Sediment. Geol. 86, 111–136. https://doi.org/10.1016/0037-0738(93)
- Schmid, S., 2017. Chemostratigraphy and palaeo-environmental characterisation of the Cambrian stratigraphy in the Amadeus Basin, Australia. Chem. Geol. 451, 169–182. https://doi.org/10.1016/j.chemgeo.2017.01.019.
- Schmid, S., Smith, P.M., Woltering, M., 2018. A basin-wide record of the late Cambrian Steptoean Positive Carbon Isotope Excursion (SPICE) in the Amadeus Basin,

- Australia. Palaeogeogr. Palaeoclimatol. Palaeoecol. 508, 116–128. https://doi.org/10.1016/j.palaeo.2018.07.027.
- Servais, T., Lehnert, O., Li, J., Mullins, G.L., Munnecke, A., Nützel, A., Vecoli, M., 2008. The ordovician biodiversification: revolution in the oceanic trophic chain. Lethaia 41, 99–109. https://doi.org/10.1111/j.1502-3931.2008.00115.x.
- Servais, T., Danelian, T., Harper, D.A.T., Munnecke, A., 2014. Possible oceanic circulation patterns, surface water currents and upwelling zones in the early Palaeozoic. GFF 136, 229–233. https://doi.org/10.1080/11035897.2013.876659.
- Servais, T., Perrier, V., Danelian, T., Klug, C., Martin, R., Munnecke, A., Nowak, H., Nützel, A., Vandenbroucke, T.R.A., Williams, M., Rasmussen, C.M.Ø., 2016. The onset of the 'Ordovician Plankton Revolution' in the late Cambrian. Palaeogeogr. Palaeoclimatol. Palaeoecol. 458, 12–28. https://doi.org/10.1016/j. palaeo.2015.11.003.
- Sial, A.N., Peralta, S., Ferreira, V.P., Toselli, A.J., Aceñolaza, F.G., Parada, M.A., Gaucher, C., Alonso, R.N., Pimentel, M.M., 2008. Upper Cambrian carbonate sequences of the argentine Precordillera and the Steptoean C-Isotope positive excursion (SPICE). Gondwana Res. 13, 437–452. https://doi.org/10.1016/J. GR.2007.05.001.
- Sial, A.N., Peralta, S., Gaucher, C., Toselli, A.J., Ferreira, V.P., Frei, R., Parada, M.A., Pimentel, M.M., Silva Pereira, N., 2013. High-resolution stable isotope stratigraphy of the upper Cambrian and Ordovician in the argentine precordillera: carbon isotope excursions and correlations. Gondwana Res. 24, 330–348. https://doi.org/10.1016/ i.gr.2012.10.014.
- Sibley, D.F., Gregg, J.M., 1987. Classification of dolomite rock textures. SEPM J. Sediment. Res. 57, 967–975. https://doi.org/10.1306/212F8CBA-2B24-11D7-8648000102C1865D
- Sloss, L.L., 1963. Sequences in the Cratonic Interior of North America. Geol. Soc. Am. Bull. 74, 93–114. https://doi.org/10.1130/0016-7606(1963)74.
- Stitt, J.H., 1975. Adaptive radiation, trilobite paleoecology, and extinction, Ptychaspid biomere, late Cambrian of Oklahoma. Fossils Strata 4, 381–390.
- Sundberg, F.A., Karlstrom, K.E., Geyer, G., Foster, J.R., Hagadorn, J.W., Mohr, M.T., Schmitz, M.D., Dehler, C.M., Crossey, L.J., 2020. Asynchronous trilobite extinctions at the early to middle Cambrian transition. Geology 48, 441–445. https://doi.org/ 10.1130/G46913.1.
- Swart, P.K., Eberli, G., 2005. The nature of the δ<sup>13</sup>C of periplatform sediments: Implications for stratigraphy and the global carbon cycle. Sediment. Geol. 175, 115–129. https://doi.org/10.1016/j.sedgeo.2004.12.029.
- Vahrenkamp, V.C., 1996. Carbon isotope stratigraphy of the Upper Kharaib and Shuaiba formations: implications for the early cretaceous evolution of the Arabian Gulf region. Am. Assoc. Pet. Geol. Bull. 80, 647–661. https://doi.org/10.1306/ 64FD8868-1724-11D7-8645000102C1865D.
- Voigt, S., Gale, A.S., Jung, C., Jenkyns, H.C., 2012. Global correlation of upper Campanian- Maastrichtian successions using carbon-isotope stratigraphy: Development of a new Maastrichtian timescale. Newsl. Stratigr. 45, 25–53. https://doi.org/10.1127/0078-0421/2012/0016.
- Wang, Z., Chen, J., Liang, T., Yuan, J., Han, C., Liu, J., Zhu, C., Zhu, D., Han, Z., 2020. Spatial variation in carbonate carbon isotopes during the Cambrian SPICE event across the eastern North China Platform. Palaeogeogr. Palaeoclimatol. Palaeoecol. 546, 109669 https://doi.org/10.1016/j.palaeo.2020.109669.
- Westberry, T., Behrenfeld, M.J., Siegel, D.A., Boss, E., 2008. Carbon-based primary productivity modeling with vertically resolved photoacclimation. Glob. Biogeochem. Cycles 22, GB2024. https://doi.org/10.1029/2007GB003078.
- Wickham, H., 2016. ggplot2: Elegant Graphics for Data Analysis. Springer-Verlag, New York. https://ggplot2.tidyverse.org.
- Wickham, H., Henry, L., 2019. tidyr: Easily Tidy Data With 'spread' and 'gather' Functions. R Package Version 0.8.3. https://CRAN.R-project.org/package=tidyr.
- Wickham, H., François, R., Henry, L., Müller, K., 2019. dplyr: A Grammar of Data Manipulation. R Package Version 0.8.3. https://CRAN.R-project.org/package=dplyr.
- Wilke, C.O., 2018. ggridges: Ridgeline plots in "ggplot2". R Package Version 0.5.1. https://CRAN.R-project.org/package=ggridges.
- ://CRAN.R-project.org/package=ggridges.

  Woods, M.A., Wilby, P.R., Leng, M.J., Rushton, A.W.A., Williams, M., 2011. The Furongian (late Cambrian) Steptoean Positive Carbon Isotope Excursion (SPICE) in Avalonia. J. Geol. Soc. Lond. 168, 851–862. https://doi.org/10.1144/0016-76492010.111
- Wotte, T., Strauss, H., 2015. Questioning a widespread euxinia for the Furongian (late Cambrian) SPICE event: indications from  $\delta^{13}$ C,  $\delta^{18}$ O,  $\delta^{34}$ S and biostratigraphic constraints. Geol. Mag. 152, 1085–1103. https://doi.org/10.1017/S0016756815000187.
- Zhao, Y., Yuan, J., Babcock, L.E., Guo, Q., Peng, J., Yin, L., Yang, X., Peng, S., Wang, C., Gaines, R.R., Esteve, J., Tai, T., Yang, R., Wang, Y., Sun, H., Yang, Y., 2019. Global standard Stratotype-section and point (GSSP) for the conterminous base of the Miaolingian Series and Wuliuan Stage (Cambrian) at Balang, Jianhe, Guizhou, China. Episodes 42, 165–184. https://doi.org/10.18814/epiiugs/2019/019013.
- Zhu, M.-Y., Zhang, J.-M., Li, G.-X., Yang, A.-H., 2004. Evolution of C isotopes in the Cambrian of China: implications for Cambrian subdivision and trilobite mass extinctions. Geobios 37, 287–301. https://doi.org/10.1016/j.geobios.2003.06.001.
- Zuo, J., Peng, S., Qi, Y., Zhu, X., Bagnoli, G., Fang, H., 2018. Carbon-isotope excursions recorded in the Cambrian system, South China: Implications for mass extinctions and sea-level fluctuations. J. Earth Sci. 29, 479–491. https://doi.org/10.1007/s12583-017-0963-x.